NAVAL POSTGRADUATE SCHOOL

MONTEREY, CALIFORNIA

THESIS

SCATTERING FROM MULTI-LAYERED METAMATERIALS USING WAVE MATRICES

by

Umit Cotuk

September 2005

Thesis Advisor:	David Jenn
Second Reader:	Michael A. Morgan

Approved for public release, distribution is unlimited

THIS PAGE INTENTIONALLY LEFT BLANK

REPORT DOCUMENTATION PAGE			Form Approved OMB No. 0704-0188
Public reporting burden for this collection of information is estimated to average 1 hour per response, including the time for reviewing instruction, searching existing data sources, gathering and maintaining the data needed, and completing and reviewing the collection of information. Send comments regarding this burden estimate or any other aspect of this collection of information, including suggestions for reducing this burden, to Washington headquarters Services, Directorate for Information Operations and Reports, 1215 Jefferson Davis Highway, Suite 1204, Arlington, VA 22202-4302, and to the Office of Management and Budget, Paperwork Reduction Project (0704-0188) Washington DC 20503.			
1. AGENCY USE ONLY ***(Leave blank)***	**2. REPORT DATE** September 2005	**3. REPORT TYPE AND DATES COVERED** Master's Thesis	
4. TITLE AND SUBTITLE: Scattering from Multi-Layered Metamaterials Using Wave Matrices			**5. FUNDING NUMBERS**
6. AUTHOR(S) Umit Cotuk			
7. PERFORMING ORGANIZATION NAME(S) AND ADDRESS(ES) Naval Postgraduate School Monterey, CA 93943-5000			**8. PERFORMING ORGANIZATION REPORT NUMBER**
9. SPONSORING /MONITORING AGENCY NAME(S) AND ADDRESS(ES) N/A			**10. SPONSORING/MONITORING AGENCY REPORT NUMBER**
11. SUPPLEMENTARY NOTES The views expressed in this thesis are those of the author and do not reflect the official policy or position of the Department of Defense or the U.S. Government.			
12a. DISTRIBUTION / AVAILABILITY STATEMENT Approved for public release, distribution is unlimited			**12b. DISTRIBUTION CODE**

13. ABSTRACT (maximum 200 words)

The complex permittivity (ε) and permeability (μ) of a material determine the response of the material to electromagnetic radiation. Usually, the real parts of ε and μ are positive for naturally occurring materials at microwave frequencies. Metamaterials are engineered media that are designed to have either a negative permittivity or permeability or both. Negative permeability and negative permittivity would cause electromagnetic waves traveling through this medium to exhibit unusual characteristics such as power flow in a direction opposite to the phase velocity. In this thesis, the wave matrix approach is used to calculate the total reflection and transmission coefficients of a multilayered structure. The method is applicable to all types of materials, including metamaterials. Several layered configurations are studied including both metamaterial and conventional dielectric layers. A MATLAB program is developed to examine the effects of frequency, angle of incidence and polarization. The results are compared to published data. Potential applications of metamaterials are also discussed.

14. SUBJECT TERMS Complex Permittivity and Permeability, Negative Index, Metamaterials			**15. NUMBER OF PAGES** 65
			16. PRICE CODE
17. SECURITY CLASSIFICATION OF REPORT Unclassified	**18. SECURITY CLASSIFICATION OF THIS PAGE** Unclassified	**19. SECURITY CLASSIFICATION OF ABSTRACT** Unclassified	**20. LIMITATION OF ABSTRACT** UL

NSN 7540-01-280-5500 Standard Form 298 (Rev. 2-89)
Prescribed by ANSI Std. 239-18

THIS PAGE INTENTIONALLY LEFT BLANK

Approved for public release, distribution is unlimited

SCATTERING FROM MULTI-LAYERED METAMATERIALS USING WAVE MATRICES

Umit Cotuk
Lieutenant Junior Grade, Turkish Navy
Electrics-Electronics Engineering, Turkish Naval Academy, 2000

Submitted in partial fulfillment of the
requirements for the degree of

MASTER OF SCIENCE IN SYSTEMS ENGINEERING

from the

NAVAL POSTGRADUATE SCHOOL
September 2005

Author: Umit Cotuk

Approved by: David Jenn
Thesis Advisor

Michael A. Morgan
Second Reader

Dan C. Boger
Chairman, Department of Information Sciences

THIS PAGE INTENTIONALLY LEFT BLANK

ABSTRACT

The complex permittivity (ε) and permeability (μ) of a material determine the response of the material to electromagnetic radiation. Usually, the real parts of ε and μ are positive for naturally occurring materials at microwave frequencies. Metamaterials are engineered media that are designed to have either a negative permittivity or permeability or both. Negative permeability and negative permittivity would cause electromagnetic waves traveling through this medium to exhibit unusual characteristics such as power flow in a direction opposite to the phase velocity. In this thesis, the wave matrix approach is used to calculate the total reflection and transmission coefficients of a multilayered structure. The method is applicable to all types of materials, including metamaterials. Several layered configurations are studied including both metamaterial and conventional dielectric layers. A MATLAB program is developed to examine the effects of frequency, angle of incidence and polarization. The results are compared to published data. Potential applications of metamaterials are also discussed.

THIS PAGE INTENTIONALLY LEFT BLANK

TABLE OF CONTENTS

THIS PAGE INTENTIONALLY LEFT BLANK

LIST OF FIGURES

LIST OF TABLES

THIS PAGE INTENTIONALLY LEFT BLANK

ACKNOWLEDGMENTS

I gratefully thank Professor David Jenn who guided this work and helped whenever I was in need of assistance. He answered all my questions patiently. Without his help, this work would not be possible. I would also like to thank Professor Michael A. Morgan for agreeing to be the second reader.

I would like to thank the Turkish Navy for giving me the opportunity to study at the Naval Postgraduate School.

Finally, I wish to thank my parents for their continuous support and encouragement.

THIS PAGE INTENTIONALLY LEFT BLANK

I. INTRODUCTION

A. BACKGROUND

For frequency domain analysis, all materials can be described electrically by their complex *permittivity* (ε) and *permeability* (μ). These parameters determine the response of the material to electromagnetic (EM) radiation. Usually, the real parts of ε and μ are both positive in naturally occurring materials. While some materials could have negative real ε (such as conductors at optical frequencies), no natural material which has a negative real μ is known. Over 30 years ago, the Russian physicist Victor Veselago predicted the existence of electromagnetic materials called metamaterials, which have negative permittivity and permeability.

Metamaterials are engineered media that are designed to have either a negative permittivity or permeability (single negative material, SNG) or both (double negative material, DNG). They are created by using composite structures that are generally periodic with periods much less than a wavelength. Negative permeability and negative permittivity would cause electromagnetic waves traveling through this medium to exhibit certain unusual characteristics. For example, waves are refracted at a negative angle relative to conventional materials. Also, due to the negative index of refraction, the phase and group velocity vectors of an electromagnetic wave are in opposite directions. These unusual properties may be used to build new devices, like highly sensitive antennas or even a perfect planar lens.

In this study, the propagation characteristics of planar multilayered structures (including both metamaterial and conventional dielectric layers) are examined using a wave matrix approach. The reflection and transmission coefficients are calculated, and applications are discussed for anti-reflection and high-reflection structures. The effects of frequency, angle of incidence and polarization are examined.

B. OBJECTIVES

The objective of this thesis is to develop a matrix approach to predict the scattering characteristics of planar multilayered structures composed of metamaterial, dielectric and magnetic layers. The wave matrix formulation is developed to calculate the

reflection and transmission coefficients of multiple layers of arbitrary thicknesses and materials. Therefore, with the help of MATLAB software, the effects of frequency, angle of incidence, polarization and layer configuration can be examined. To validate the MATLAB program, many test cases are presented and simulation results are compared to published data.

C. ORGANIZATION OF THESIS

In Chapter II, equations for transmission and reflection coefficients for a single boundary between two dielectric media are presented. The wave matrix approach for layered media is described. The reflection and transmission coefficient equations are given for layered media.

In Chapter III, metamaterials and their unusual characteristics are discussed. The potential applications of DNG materials are presented.

In Chapter IV, the propagation characteristics of multilayered structures consisting of dielectric slabs, metamaterials, or both, are discussed. Different methods are described to achieve zero reflection or high reflection. The effects of frequency, angle of incidence and polarization are shown. The potential applications of these structures are described.

Finally in Chapter V, the results, conclusions and suggestions for future studies are discussed.

II. WAVE REFLECTION AND TRANSMISSION

A. INTRODUCTION

Electric charges generate electric fields and electric currents generate magnetic fields. If the charge and currents sources were to vary with time, the electric and magnetic fields become unified, and the link between them generates electromagnetic waves (EM) that can travel through free space and in material media. If a plane wave from one medium meets a different medium, it is partly reflected and partly transmitted depending on the constitutive parameters of the two media involved. This chapter begins with an examination of the reflection and transmission properties of plane waves incident on planar boundaries, and continues with the development of wave matrices for layered media.

B. REFLECTION AND TRANSMISSION COEFFICIENTS

Consider a uniform plane wave traveling along the +z-direction that is normally incident at the boundary between medium 1 (μ_1, ε_1) and medium 2 (μ_2, ε_2). The incident (i), reflected (r), and transmitted (t) waves are shown in Figure 1.

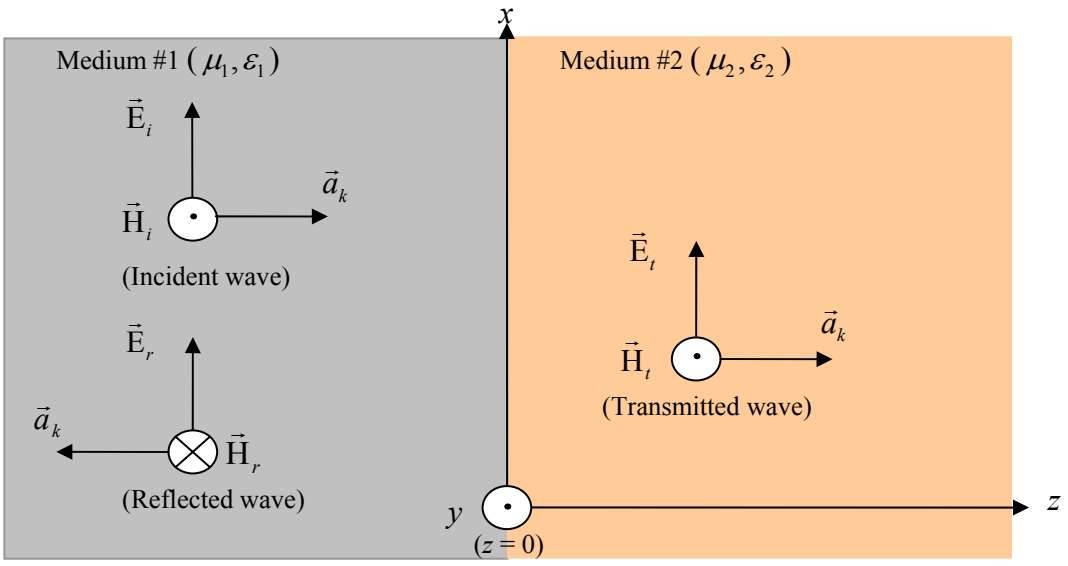

Figure 1. A plane wave incident normally on an interface between two different media (After Ref. [1]).

The incident wave is traveling in the $+z$ direction in medium 1. For normal incidence, the incident electric field vector can be expressed as

$$\vec{\mathrm{E}}_i(z) = \mathrm{E}_{i0} e^{-\gamma_1 z} \vec{a}_x \tag{2.1}$$

and the magnetic field vector

$$\vec{\mathrm{H}}_i(z) = \mathrm{H}_{i0} e^{-\gamma_1 z} \vec{a}_y = \frac{\mathrm{E}_{i0}}{\eta_1} e^{-\gamma_1 z} \vec{a}_y \tag{2.2}$$

where η_1 is *intrinsic impedance* of material 1, given as

$$\eta_1 = \sqrt{\frac{\mu_1}{\varepsilon_1}} = \sqrt{\frac{\mu_0}{\varepsilon_0}} \sqrt{\frac{\mu_{r_1}}{\varepsilon_{r_1}}} \tag{2.3}$$

and $\mu_{r_1} = \mu_{r_1}' - j\mu_{r_1}''$, $\varepsilon_{r_1} = \varepsilon_{r_1}' - j\varepsilon_{r_1}''$ are the relative *permeability* and *permittivity* of the medium. Also, γ_1 is the *propagation constant* of the medium, and is given as

$$\gamma_1 = \alpha_1 + j\beta_1 = \omega\sqrt{\mu_0 \varepsilon_0} \sqrt{\mu_{r_1} \varepsilon_{r_1}} \,. \tag{2.4}$$

The reflected wave is traveling in the $-z$ direction in medium 1. The reflected electric field vector can be written as

$$\vec{\mathrm{E}}_r(z) = \mathrm{E}_{r0} e^{\gamma_1 z} \vec{a}_x \tag{2.5}$$

and the magnetic field vector is

$$\vec{\mathrm{H}}_r(z) = \mathrm{H}_{r0} e^{\gamma_1 z} (-\vec{a}_y) = -\frac{\mathrm{E}_{i0}}{\eta_1} e^{\gamma_1 z} \vec{a}_y \,. \tag{2.6}$$

The transmitted wave is traveling in the $+z$ direction in medium 2, and its electric field vector is

$$\vec{\mathrm{E}}_t(z) = \mathrm{E}_{t0} e^{-\gamma_2 z} \vec{a}_x \tag{2.7}$$

and its magnetic field vector

$$\vec{\mathrm{H}}_t(z) = \mathrm{H}_{t0} e^{-\gamma_2 z} \vec{a}_y = \frac{\mathrm{E}_{i0}}{\eta_2} e^{-\gamma_2 z} \vec{a}_y \tag{2.8}$$

where η_2 and γ_2 are defined in manner similar to Equations (2.3) and (2.4).

In Figure 1, the total field in medium 1 includes both the incident and reflected fields. In medium 2, only the transmitted field is present. Then, the total fields can be written as

$$\begin{aligned} \vec{\mathrm{E}}_1 &= \vec{\mathrm{E}}_i + \vec{\mathrm{E}}_r \\ \vec{\mathrm{H}}_1 &= \vec{\mathrm{H}}_i + \vec{\mathrm{H}}_r \\ \vec{\mathrm{E}}_2 &= \vec{\mathrm{E}}_t \\ \vec{\mathrm{H}}_2 &= \vec{\mathrm{H}}_t. \end{aligned}$$

The planar boundary located at z=0 separates the two media. At the boundary, the tangential components of the electric and magnetic fields are continuous. Thus,

$$\mathrm{E}_{1t} = \mathrm{E}_{2t} \rightarrow \mathrm{E}_{i0} + \mathrm{E}_{r0} = \mathrm{E}_{t0} \tag{2.9}$$

$$\mathrm{H}_{1t} = \mathrm{H}_{2t} \rightarrow \mathrm{H}_{i0} + \mathrm{H}_{r0} = \mathrm{H}_{t0} \rightarrow \frac{(\mathrm{E}_{i0} - \mathrm{E}_{r0})}{\eta_1} = \frac{\mathrm{E}_{t0}}{\eta_2}. \tag{2.10}$$

From Equations (2.9) and (2.10),

$$\mathrm{E}_{r0} = \frac{\eta_2 - \eta_1}{\eta_2 + \eta_1} \mathrm{E}_{i0} \tag{2.11}$$

$$\mathrm{E}_{t0} = \frac{2\eta_2}{\eta_2 + \eta_1} \mathrm{E}_{i0}. \tag{2.12}$$

Now it is possible to obtain the *reflection coefficient* (Γ) and *transmission coefficient* (τ) from Equations (2.11) and (2.12),

$$\Gamma = \frac{\mathrm{E}_{r0}}{\mathrm{E}_{i0}} = \frac{\eta_2 - \eta_1}{\eta_2 + \eta_1} \tag{2.13}$$

$$\tau = \frac{\mathrm{E}_{t0}}{\mathrm{E}_{i0}} = \frac{2\eta_2}{\eta_2 + \eta_1}. \tag{2.14}$$

To simplify the analysis, normal incidence is assumed. Situations that are more general are considered in the following chapters.

C. WAVE MATRICES FOR LAYERED MEDIA

Thus far, the focus has been on uniform plane waves traveling through two media and a single boundary. next, a more complex situation is considered; that is, multilayered media. First, the two-media equations are rewritten in matrix form and then the matrix is extended for N layers.

Figure 2 shows incident waves approaching the boundary from both sides (traveling in the $+z$ and $-z$ directions), and waves traveling away from the boundary in both media. By denoting the $+z$ traveling incident wave b_1, and $-z$ traveling incident

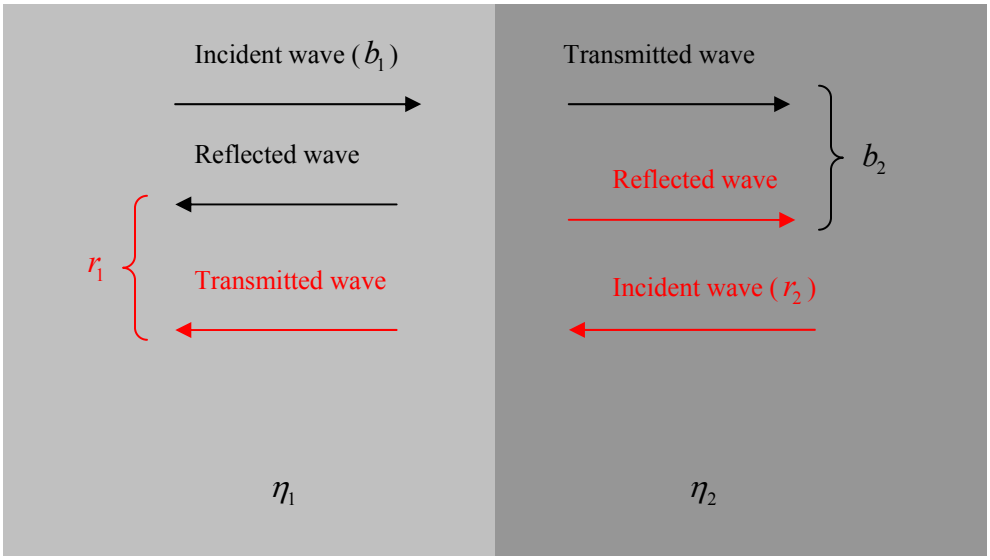

Figure 2. Normal incidence at a boundary between two media.

wave r_2, then incident waves become,

$$r_1 = \Gamma_1 b_1 + \tau_{21} r_2 \tag{2.15}$$

and

$$b_2 = \Gamma_2 r_2 + \tau_{12} b_1 \tag{2.16}$$

where the first subscript on τ denotes the incident medium and the second subscript denotes the transmitted medium. Now it is possible to rearrange Equations (2.15) and (2.16), and write them in the matrix form [Ref. 2],

$$\begin{bmatrix} b_1 \\ r_1 \end{bmatrix} = \frac{1}{\tau_{12}} \begin{pmatrix} 1 & -\Gamma_2 \\ \Gamma_1 & \tau_{12}\tau_{21} - \Gamma_1\Gamma_2 \end{pmatrix} \begin{bmatrix} b_2 \\ r_2 \end{bmatrix}. \tag{2.17}$$

The wave matrix in Equation (2.17) is for a two-layered structure. Next, it will be extended to N layers. Figure 3 shows forward (+z) and backward (-z) traveling waves through the N layers.

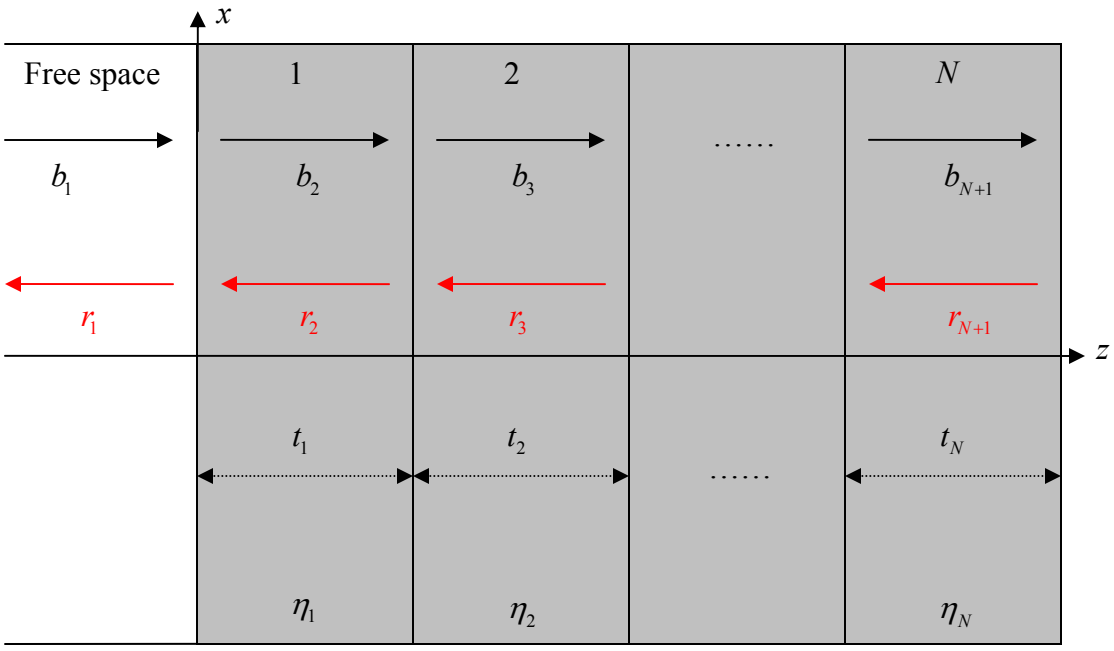

Figure 3. Forward and backward traveling waves through N layers (After Ref. [2]).

To simplify the equations, the forward traveling waves are named $b_1, b_2, ..., b_N$ and the backward traveling waves are named $r_1, r_2, ..., r_N$. At $z = t_1$, the forward traveling wave becomes $b_1 e^{-j\gamma_1 t_1}$, and backward traveling wave becomes $r_1 e^{j\gamma_1 t_1}$, where γ_n is the propagation constant for layer n defined in Equation (2.4)

$$\gamma_n = \frac{\omega}{c}\sqrt{\mu_{r_n}\varepsilon_{r_n}} = \frac{2\pi}{\lambda}\sqrt{\mu_{r_n}\varepsilon_{r_n}} \tag{2.18}$$

where λ is the wavelength in the free space.

For the plane wave in Figure 3, traveling from free space through the *N*-layered medium, the wave matrices can be cascaded to give

$$\begin{bmatrix} b_1 \\ r_1 \end{bmatrix} = \prod_{n=1}^{N} \frac{1}{\tau_n} \begin{pmatrix} e^{\gamma_n t_n} & \Gamma_n e^{-\gamma_n t_n} \\ \Gamma_n e^{\gamma_n t_n} & e^{-\gamma_n t_n} \end{pmatrix} \begin{bmatrix} b_{N+1} \\ r_{N+1} \end{bmatrix} \equiv \begin{pmatrix} a_{11} & a_{12} \\ a_{21} & a_{22} \end{pmatrix} \begin{bmatrix} b_{N+1} \\ r_{N+1} \end{bmatrix}. \tag{2.19}$$

If the thickness of the last layer of the medium extends to ∞, then it is possible to state that $b_{N+1} = 0$. The total transmission and reflection coefficients of the medium become,

$$\tau_T = \frac{b_{N+1}}{b_1} = \frac{1}{a_{11}} \tag{2.20}$$

$$\Gamma_T = \frac{r_1}{b_1} = \frac{a_{21}}{a_{11}}. \tag{2.21}$$

Thus far, the equations in this chapter are based on normal incidence. The wave matrix can be extended to non-normal angles by using the wave impedance in place of the intrinsic impedance. The normalized wave impedance for a parallel-polarized wave incident at an angle θ_i from the interface normal is given as [3]

$$Z = \frac{\sqrt{\varepsilon_r \mu_r - \sin^2 \theta_i}}{\varepsilon_r \cos \theta_i} \tag{2.22}$$

and for a perpendicularly-polarized wave

$$Z = \frac{\mu_r \cos \theta_i}{\sqrt{\varepsilon_r \mu_r - \sin^2 \theta_i}}. \tag{2.23}$$

The transmission and reflection coefficients at the interface between the two media are given as

$$\Gamma = \frac{Z_2 - Z_1}{Z_2 + Z_1} \tag{2.24}$$

$$\tau = 1 + \Gamma \tag{2.25}$$

where Z_1 is the incidence medium and Z_2 is the transmitted medium. Finally, the phase of the layer (thickness *t*) is given as

$$\Phi = \frac{2\pi}{\lambda} t\sqrt{\varepsilon_r \mu_r - \sin^2 \theta_i} \ . \tag{2.26}$$

D. SUMMARY

The first part of this chapter presented the equations for transmission and reflection coefficients. These equations are based on normal incidence, and a single boundary between two dielectric media.

The second part described wave matrices for layered media. Then, reflection and transmission coefficient equations are given, both for parallel-polarized and perpendicularly-polarized waves incident at an angle θ_i. These situations are simulated with MATLAB 6.5 in Chapter IV, both for dielectric media and metamaterials. However, first a brief description of metamaterials is given.

THIS PAGE INTENTIONALLY LEFT BLANK

III. METAMATERIALS

A. INTRODUCTION

In 1968, Victor Veselago (a Russian physicist) forecasted the existence of a material in which both permittivity and permeability were assumed to have negative real values (negative index of refraction) [4]. These materials have been called metamaterials, backward-wave materials and left-handed (LH) materials. Although these materials were not known to exist at that time, he concluded that with these negative-index materials all known wave propagation and optical behaviors would be changed.

Materials with negative permittivity occur naturally (e.g., metals at optical frequencies), but those with negative permeability do not. Victor Veselago's prediction was verified after more than 30 years when in 1999, John Pendry (Imperial College, London) showed how these materials could be created artificially [4]. Then, in the following year, he published a paper in which he proposed that metamaterials could be used to make a perfect lens [5].

B. NEGATIVE PERMITTIVITY AND PERMEABILITY

Metamaterials are created by using composite structures which are engineered to have properties that do not occur naturally. Figure 4 shows one type of negative-index material that was constructed by David Smith at the University of California in 2000 [4].

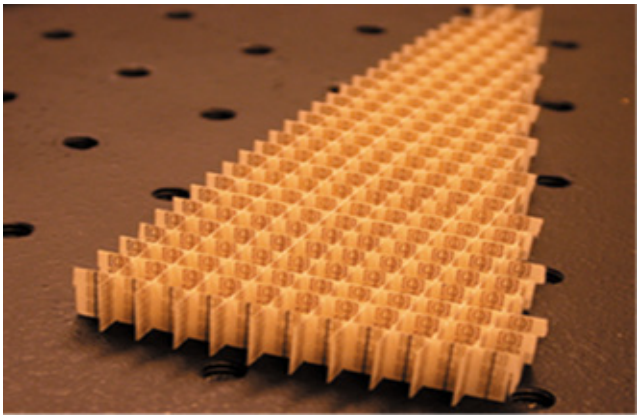

Figure 4. An artificial negative-index material made from grids of rings and wires (From Ref. [4]).

The cells are small compared to the wavelength so that macroscopically the effective index of refraction is negative.

Metamaterials are engineered media that are designed to have either a negative permittivity or permeability (SNG) or both (DNG). For a DNG material, the index of refraction for real permittivity and permeability is

$$n = -\sqrt{|\mu_r||\varepsilon_r|}\,,\ \mu_r < 0, \varepsilon_r < 0 \tag{3.1}$$

and the intrinsic impedance

$$\eta = \eta_0 \sqrt{|\mu_r|/|\varepsilon_r|}\,. \tag{3.2}$$

They have several unusual properties when compared to the regular materials [6]:

1. The phase velocity of EM waves is anti-parallel to the group velocity and the flow of the energy. Thus, propagation is described by a left-hand rule.
2. Waves are refracted at a negative angle relative to conventional materials.
3. Evanescent waves grow with distance into the medium.
4. The Doppler shift is reversed and Cerenkov radiation propagates backwardly.

Artificial materials are a mix of regular materials combined to obtain specific characteristics. A negative ε_r' can be obtained by a three dimensional array of wires [7] (Figure 5). The effective dielectric constant is given as

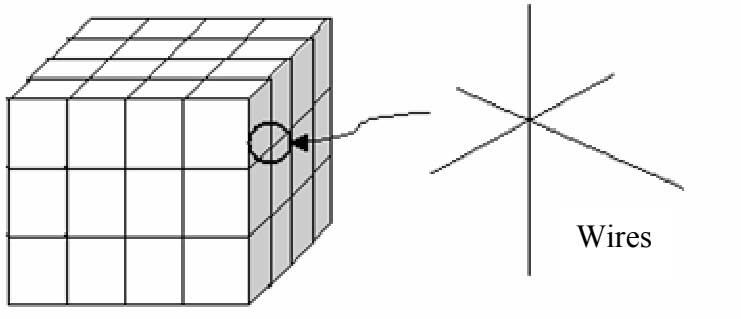

Figure 5. Three-dimensional grid of thin wires approximates a plasma (From Ref. [7]).

$$\varepsilon_{r_{eff}} = 1 - \frac{\omega_p{}^2}{\omega\left(\omega + \frac{j\varepsilon_0 a^2 \omega_p{}^2}{\pi\sigma r^2}\right)} \tag{3.3}$$

where $\omega_p = \frac{2\pi c^2}{a^2 \ln(a/r)}$, r is the radius of the wire, a is the grid spacing and σ is the wire conductivity.

A coplanar ring (CPR) is an example of a configuration that influences both the effective permittivity and permeability of a material (Figure 6). The effective permeability of the CPR is given as

$$\mu_{eff} = 1 - \frac{\pi r^2 / a^2}{1 + j\frac{2\ell\rho}{\omega r \mu_0} - \frac{3}{\pi^2 \omega^2 \mu_0 C r^3}} \tag{3.4}$$

where ρ is the resistivity of the metal (ohms/m), $C = \frac{\varepsilon_0}{\pi}\ln\left(\frac{2s}{t}\right)$ is the capacitance per meter of two parallel strips, $a =$ lattice spacing in the plane of rings and $\ell =$ spacing between sheets of rings.

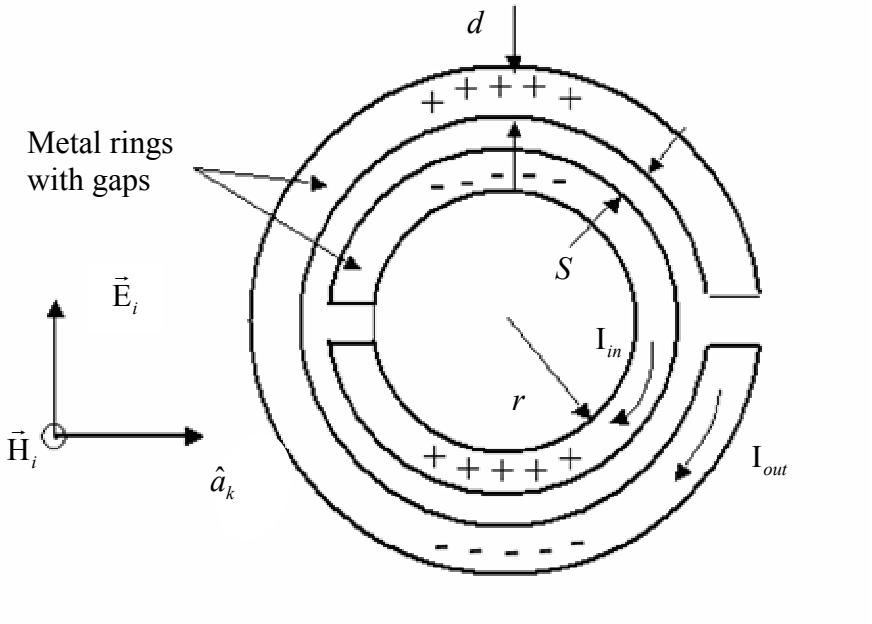

Figure 6. Coplanar ring (From Ref. [7]).

1. Left Hand Rule

All materials can be described electrically by an equivalent complex *permittivity* and *permeability*. The permittivity of a material ($\varepsilon = \varepsilon_0 \varepsilon_r$) determines its response to an electric field, while permeability ($\mu = \mu_0 \mu_r$) determines its response to a magnetic field. Together these two parameters determine the reaction of the material to the EM radiation. All natural (passive) materials follow a right-hand (RH) rule because of their positive values of relative permittivity and permeability. However, the double negative-index materials follow the left-hand (LH) rule [6]. Figure 7 demonstrates these rules where $\vec{S}$ is the poynting vector defined as

$$\vec{S}=\vec{E}\times\vec{H}^{*}. \tag{3.5}$$

A material for which the RH rule holds is called right-handed material (RHM). The LH rule holds in a left-handed material (LHM). In a LHM, the phase of the waves (given by vector $\vec{a}_k$) moves in the direction opposite to the direction of the energy flow (given by vector $\vec{S}$) .

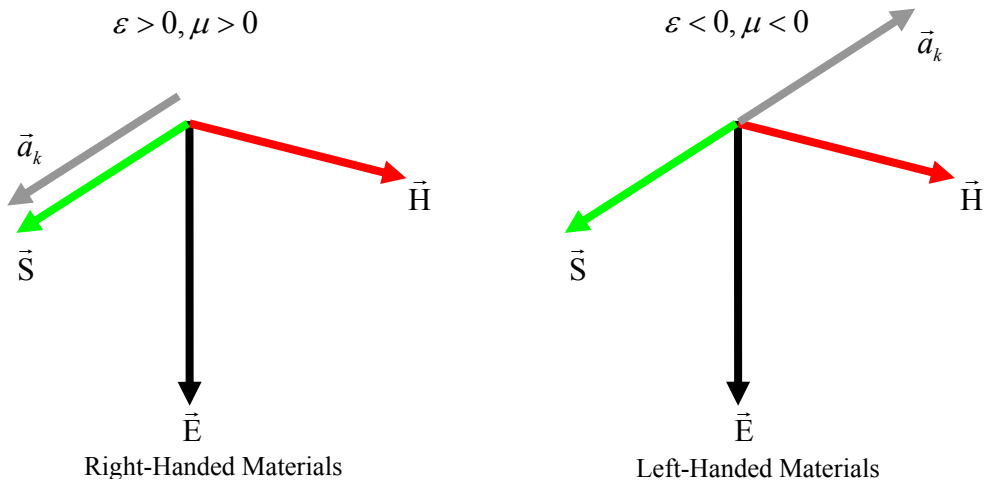

Figure 7. Illustration of vector relationships for right-hand and left-hand rules.

2. Negative Refraction

Snell's law gives the relationship between angles of incidence and refraction at an interface between two media with different indices of refraction

$$n_1 \sin\theta_1 = n_2 \sin\theta_2 . \tag{3.6}$$

The same law applies for negative-index materials, but because of the negative sign, the refracted wave remains on the same side of the normal as the incident wave. In Figure 8, a wave that strikes an interface between air and a positive-index material is refracted towards the surface normal, while in a negative index material, it is refracted on the opposite side.

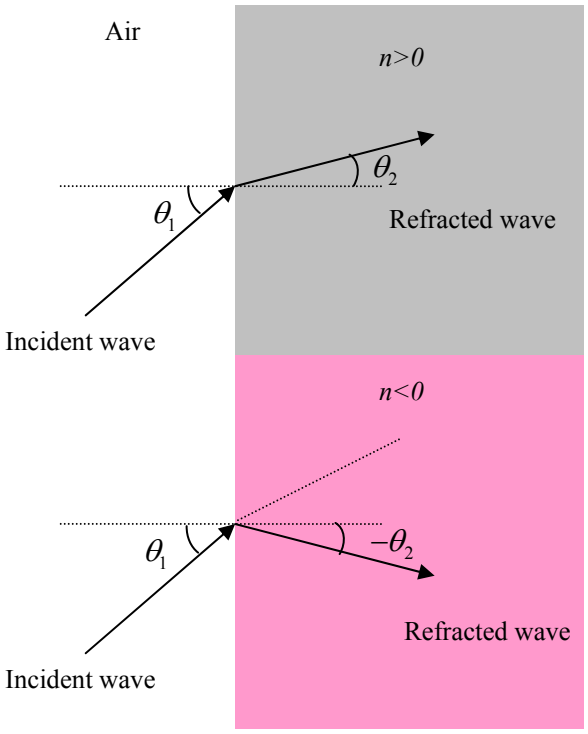

Figure 8. Refraction in a positive-index material (top), and in a negative-index material (bottom).

Measurements and simulations with artificial negative-index materials have been performed. In Figure 9, an experiment at MTI has shown the predicted refraction behavior [8]. The index of refraction of Teflon and a LHM are determined at 10.5 GHz by measuring the angle of refraction. The propagation is toward the top of the figure and the beam is normally incident on the prisms. The opposite faces of prisms are cut at an angle of 18°. To prevent leakage out of the sides, absorbing foam is used in the lower half of the figures. The measured indices were $n = 1.52 \pm 0.07$ for Teflon (actual index for Teflon, $n = 1.5$) with a refraction angle of $\theta = 28° \pm 2°$ and $n = -0.36 \pm 0.13$. For the left-handed material, the measured refraction angle was $\theta = -6.4° \pm 2.4°$. A microwave beam

traveling upwards is refracted in the positive direction when it leaves a Teflon wedge, while it is refracted in the opposite direction when it leaves a metamaterial prism constructed from wires and rings. Two lobes appear in the LHM prism due to the corrugation of the refractive surface.

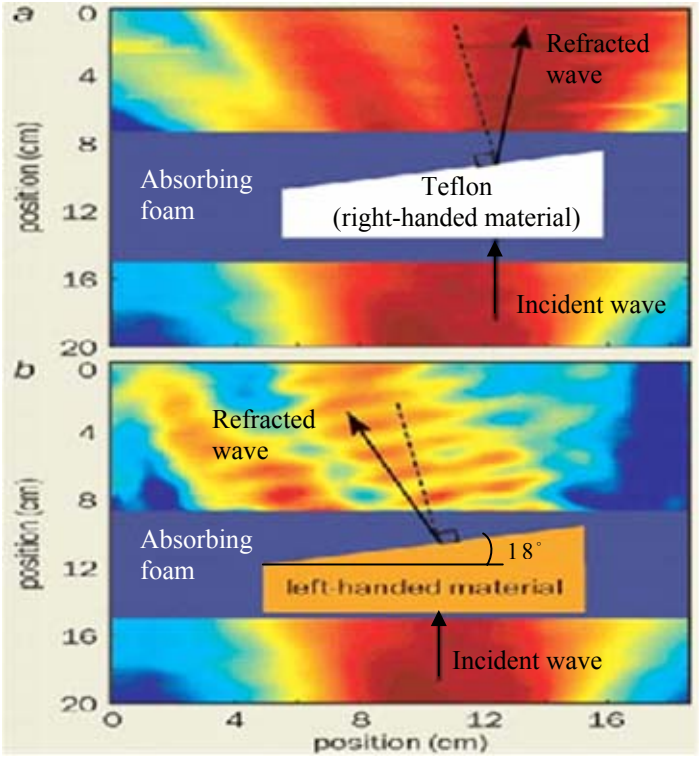

Figure 9. A microwave beam refracted in Teflon (a), and refracted in a metamaterial (b) (From Ref. [8]).

In theory, a negative refraction material can be used to build a completely flat lens that focuses light to a point (Pendry's perfect lens [5]). Instead of making specific concave or convex surfaces, metamaterials should be able to serve as a perfect lens with a simple plane surface. Unlike standard lenses, metamaterial lenses have no optical axis. Figure 10 demonstrates the idea of a planar metamaterial lens.

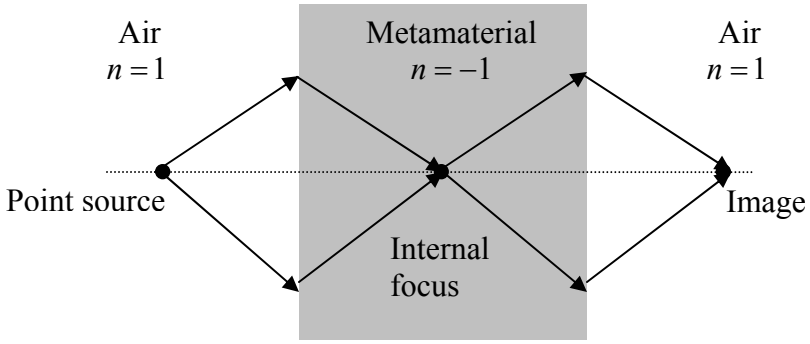

Figure 10. Planar metamaterial lens, known as Pendry's perfect lens (After Ref. [5]).

3. Growing Evanescent Waves

Evanescent waves are formed when sinusoidal waves are internally reflected off an interface at an angle greater than the critical angle. In a RHM, the evanescent waves decay exponentially in amplitude with distance from the interface at which they are formed. Left-handed materials can cancel the decay of evanescent waves [5]. Pendry showed that evanescent waves emerge from the far side of the medium enhanced in amplitude by the transmission process [5]. This does not violate energy conservation because evanescent waves do not carry energy.

4. Reversed Doppler and Cerenkov Radiation

The Doppler Effect is the apparent change in frequency or wavelength of a wave that is received by an observer moving relative to the source of the waves. The relation between the actual frequency (f_0) and observed frequency (*f*) for a moving target is given as

$$f = f_0\left(1+\frac{v_o}{v}\right) \tag{3.7}$$

where v is the speed of the waves in the medium and v_o is the speed of the observer (positive towards the source and negative if moving away). This yields an increase in the observed frequency if the observer is moving towards the source. If the propagation medium is a LHM, this effect is reversed due to the anti-parallel phase velocity [6].

Cherenkov radiation is EM radiation emitted when a charged particle moves at a speed greater than that of light in the medium. The radiation propagates in the forward direction in a RHM. In a LHM, radiation flows backward, opposite to the particle velocity [6].

C. APPLICATIONS OF DNG MATERIALS

Negative-index materials have attracted great attention recently. It may be possible to build new devices by using metamaterials, like new antenna configurations or perfect planar lenses. Some possible applications of metamaterials are [4]:

1. Highly sensitive antennas.
2. Phase and dispersion compensation phase shifters.
3. Antenna and microwave-device miniaturization.
4. Broadband and multi-band antenna design.
5. Planar lenses that exceed the diffraction limit.

The list above includes only a few examples among the possible applications. As the new properties of metamaterials are discovered, the list is likely to be extended.

IV. ANALYSIS OF SCATERING FROM MULTI-LAYERED METAMATERIALS

A. INTRODUCTION

In this chapter, the wave matrix approach is used to calculate the reflection and transmission coefficients of multilayered structures, including both metamaterial and dielectric layers. These equations were programmed in MATLAB 6.5 so that the effects of frequency, angle of incidence and polarization could be examined.

B. MATLAB SOFTWARE AND SIMULATIONS

1. Lossless Dielectric Panel

The first configuration considered is a single dielectric slab. Figure 11 shows a dielectric panel that has a thickness of $t = 0.1$ m and a relative dielectric constant of $\varepsilon_r = 4$.

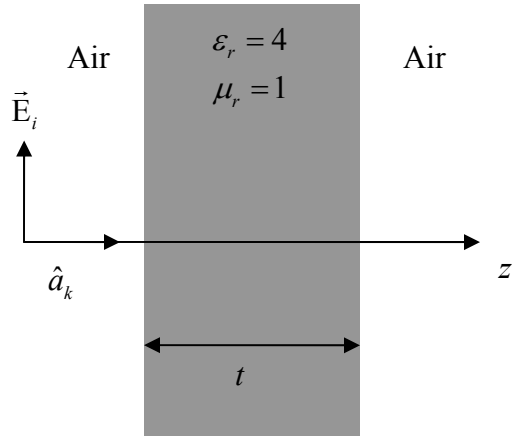

Figure 11. Dielectric panel with thickness t and permittivity $\varepsilon = 4\varepsilon_0$.

Assuming normal incidence, from Equations (2.13) and (2.14), the reflection and transmission coefficients become [2],

$$\Gamma_1 = \frac{\eta_1 - \eta_0}{\eta_1 + \eta_0} = \frac{\sqrt{\frac{\mu_r}{\varepsilon_r}} - 1}{\sqrt{\frac{\mu_r}{\varepsilon_r}} + 1} = \frac{\frac{1}{\sqrt{4}} - 1}{\frac{1}{\sqrt{4}} + 1} = -\frac{1}{3} \tag{4.1}$$

$$\tau_1 = 1 + \Gamma_1 = \frac{2}{3} \tag{4.2}$$

and

$$\Gamma_2 = \frac{\eta_0 - \eta_1}{\eta_0 + \eta_1} = \frac{1 - \frac{1}{\sqrt{4}}}{1 + \frac{1}{\sqrt{4}}} = \frac{1}{3} \tag{4.3}$$

$$\tau_2 = 1 + \Gamma_2 = \frac{4}{3}. \tag{4.4}$$

It is also possible to write the wave matrix for the panel by using Equation (2.19). First, Figure 11 is redrawn to show the incident and reflected waves, as shown in Figure 12. Now, the wave matrix becomes

$$\begin{bmatrix} b_1 \\ r_1 \end{bmatrix} = \prod_{n=1}^{2} \frac{1}{\tau_n} \begin{pmatrix} e^{j\Phi_n} & \Gamma_n e^{-j\Phi_n} \\ \Gamma_n e^{j\Phi_n} & e^{-j\Phi_n} \end{pmatrix} \begin{bmatrix} b_3 \\ r_3 \end{bmatrix} \tag{4.5}$$

where $\Phi_n = \gamma_n t_n$. Since the thickness of the last layer (t_2) extends to ∞, it is possible to arbitrarily state that $r_3 = 0$ and $\Phi_2 = 0$. Then, is obtained,

$$\begin{bmatrix} b_1 \\ r_1 \end{bmatrix} = \begin{pmatrix} e^{j\Phi_1} & \Gamma_1 e^{-j\Phi_1} \\ \Gamma_1 e^{j\Phi_1} & e^{-j\Phi_1} \end{pmatrix} \begin{pmatrix} 1 & \Gamma_2 \\ \Gamma_2 & 1 \end{pmatrix} \begin{bmatrix} b_3 \\ r_3 \end{bmatrix}. \tag{4.6}$$

The panel transmission and reflection coefficients as a function of frequency are plotted for the range of 500 MHz to 2 GHz in Figure 13. As evident in Figure 13, the slab has minimum reflection (maximum transmission) coefficients at 0.75 and 1.5 GHz. These are the frequencies where the thickness is a multiple of $\lambda/2$, where λ is wavelength in the dielectric.

Figure 14 shows the transmission and reflection coefficients for parallel polarization at various angles of incidence when the frequency is 2 GHz. The slab has a minimum reflection coefficient at $\theta_i = 64^\circ$, which is the Breuster's angle.

When the wave is perpendicularly polarized, the slab has its minimum reflection coefficient at $\theta_i = 0^\circ$. In this case, high-reflection is observed at grazing angles (Figure 15).

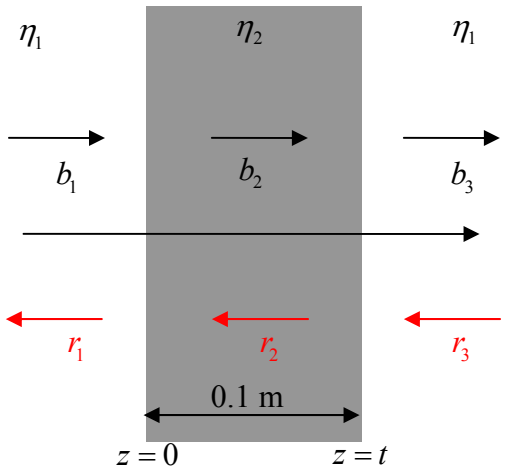

Figure 12. Incidence and traveling waves in a lossless dielectric panel (After Ref. [2]).

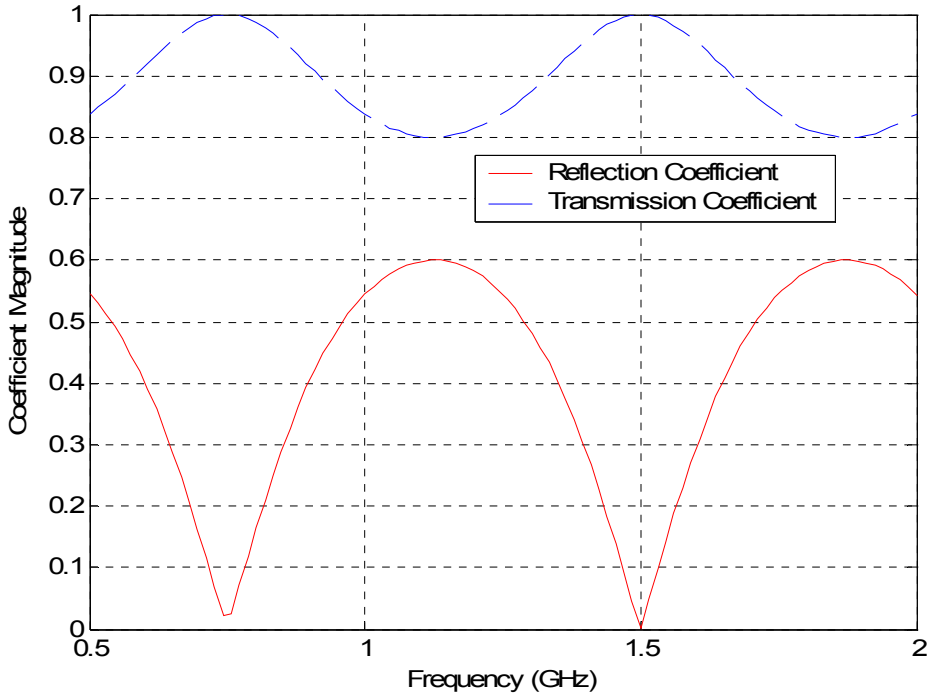

Figure 13. Transmission and reflection coefficients of a lossless dielectric slab with $\varepsilon_r = 4$ as a function of frequency (normal incidence, parallel polarization).

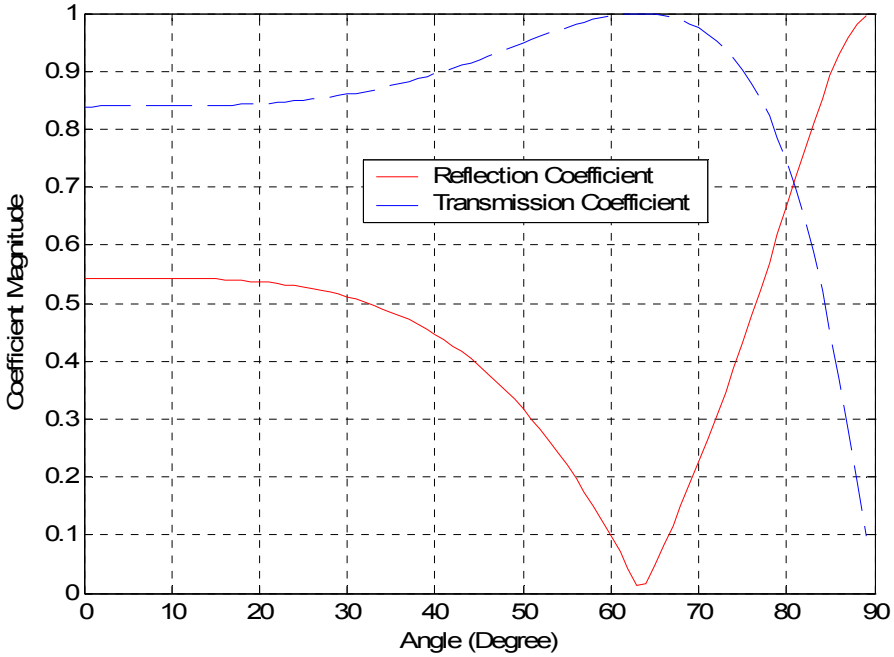

Figure 14. Transmission and reflection coefficients of a lossless dielectric slab as a function of incidence angle ($f = 2$ GHz, parallel polarization).

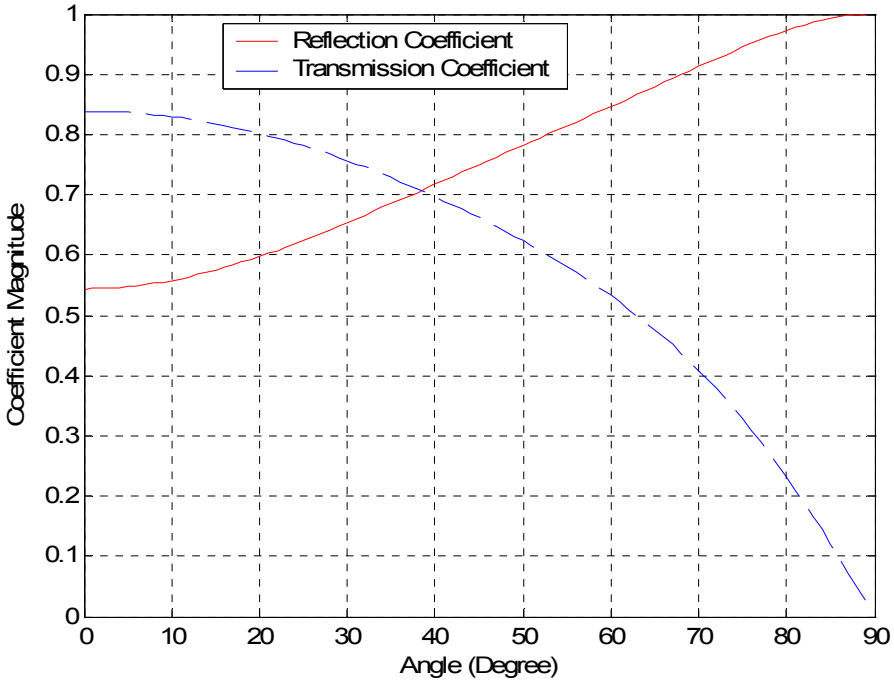

Figure 15. Transmission and reflection coefficients of a lossless dielectric slab as a function of incidence angle ($f = 2$ GHz, perpendicular polarization).

2. Radar Absorbing Material

There are several methods of reducing the RCS (radar cross section) of targets. Radar absorbing materials (RAM) is one of them. The next case examined is a combination of dielectric and magnetic material used in RAM applications. The proper thickness, material configuration and electromagnetic parameter values of a single layer RAM over a perfect conductor can produce zero specular reflection. There are two different approaches to achieve zero specular reflection [9]. The first is the *matched characteristic impedance* method, in which the characteristic impedance of the material is made equal to the characteristic impedance of the free space. The second is the *matched wave impedance* method, in which the wave impedance of the material is made equal to that of free space.

Figure 16 shows a set of *universal curves* for RAM design based on the matched wave impedance method. There are six independent parameters incorporated in the universal curves: $t, \lambda, \mu_r', \mu_r'', \varepsilon_r'$ and ε_r''. They can be reduced to four by normalizing permittivity and permeability by t/λ. Define the following:

$$\begin{aligned} x &= (t/\lambda)\,\mathrm{Re}[\mu] = (t/\lambda)\mu_r' \\ y &= (t/\lambda)\,\mathrm{Im}[\mu] = (t/\lambda)\mu_r' \\ a &= (t/\lambda)\,\mathrm{Re}[\varepsilon] = (t/\lambda)\varepsilon_r' \\ b &= (t/\lambda)\,\mathrm{Im}[\varepsilon] = (t/\lambda)\varepsilon_r''. \end{aligned} \tag{4.7}$$

In Figure 16, red lines represent values of a and blue lines represent values of $\tan\delta_e$, where $\tan\delta_e = a/b$. To enter the chart, a and the loss tangent ($\tan\delta_e$) are needed. Then, it is possible to find the sets of x and y for zero reflection by using the chart.

As an example, a design of a RAM layer at 10 GHz with a maximum thickness of 3 mm is proposed. If the layer is comprised of a dielectric with $\varepsilon_r' = 10$ and $\varepsilon_r'' = 100$, it is possible to use the universal curves to determine μ_r' and μ_r''. To enter the chart, it is necessary to find a and the electric loss tangent. By using Equation (4.7),

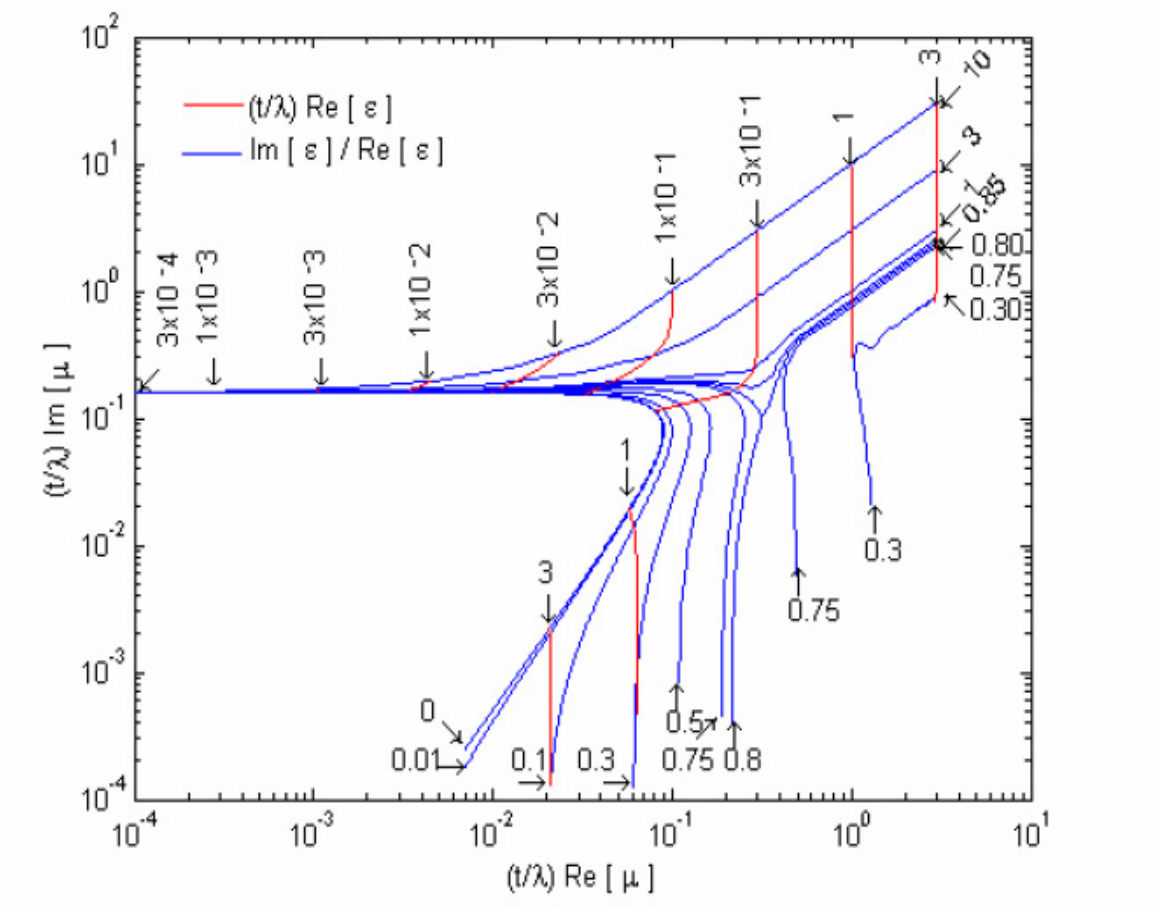

Figure 16. Universal curves for zero specular reflection (From Ref. [6]).

$$\lambda = c/f = 0.03\ \text{m} \rightarrow \frac{t}{\lambda} = 0.1 \tag{4.8}$$

$$a = \frac{t}{\lambda}\varepsilon_r' = (0.1)(10) = 1 \tag{4.9}$$

$$\tan\delta_e = a/b = \frac{\varepsilon_r''}{\varepsilon_r'} = 10\,. \tag{4.10}$$

By going to the intersection of curves for these values of a and $\tan\delta_e$, it is then possible to determine x and y:

$$x = \frac{t}{\lambda}\mu_r' \approx 1 \rightarrow \mu_r' \approx 10 \tag{4.11}$$

$$y = \frac{t}{\lambda}\mu_r'' \approx 1 \rightarrow \mu_r'' \approx 100 \tag{4.12}$$

$$\mu_r = \mu' - \mu'' = 10 - j100 . \tag{4.13}$$

This is a matched characteristic impedance case where $\varepsilon_r = \mu_r$. In general, the upper part of the chart represents the matched characteristic impedance absorbers.

Now, to demonstrate the zero specular reflection, the reflection and transmission coefficients of the RAM designed by using the universal curve using the wave matrix formulation will be plotted. Figure 17 shows reflection and transmission coefficients of the RAM as a function of angle of incidence for a parallel polarized wave. From normal incidence up to $\theta_i = 35°$, the reflection coefficient is smaller than 0.1.

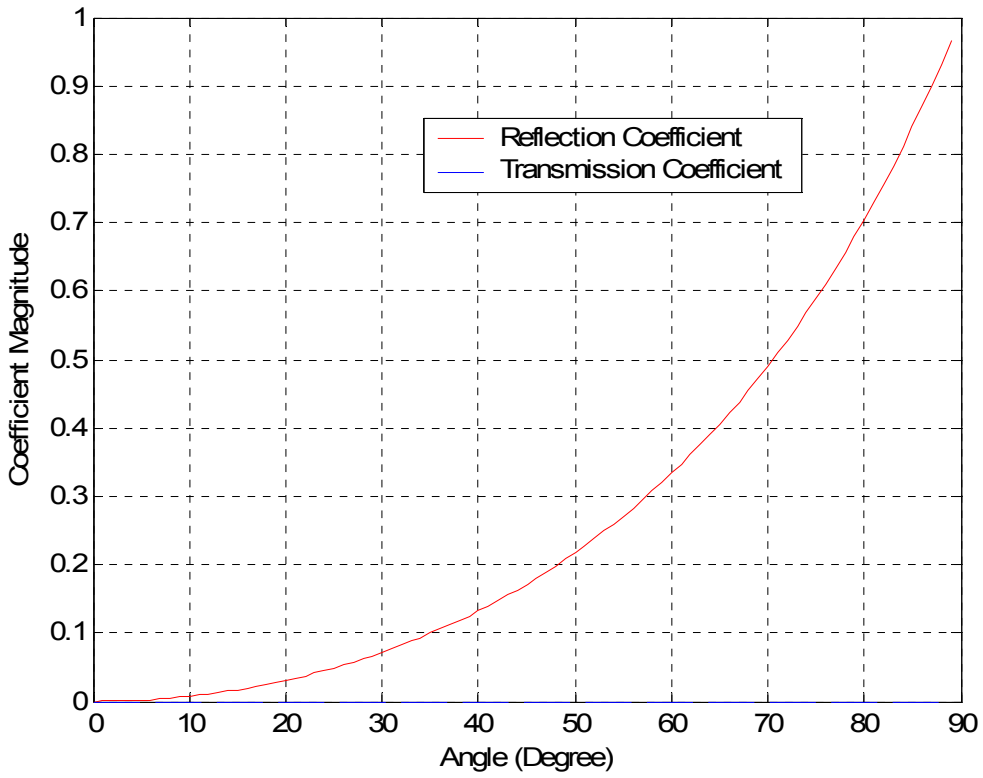

Figure 17. Transmission and reflection coefficients of a RAM layer as a function of angle of incidence (parallel polarization).

Figure 18 shows the reflection and transmission coefficients of the RAM layer for a perpendicularly polarized wave. As evident in the figure, coefficients are polarization independent because $\mu_r = \varepsilon_r$ in the material.

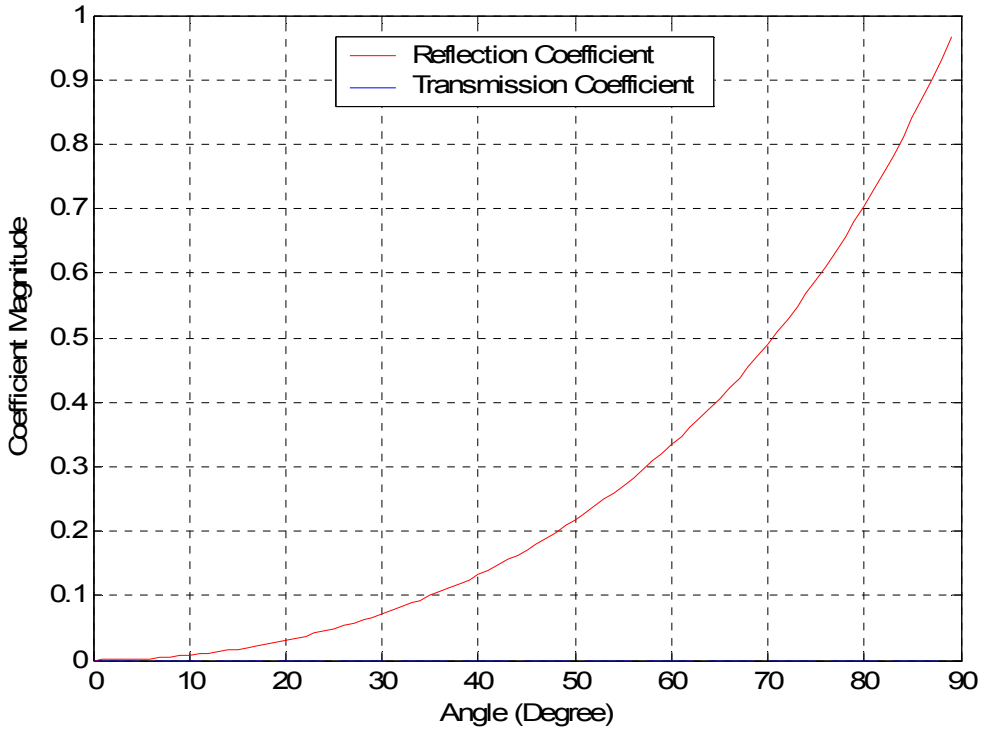

Figure 18. Transmission and reflection coefficients of a RAM layer as a function of angle of incidence (perpendicular polarization).

3. Propagation in Metamaterial Slabs

The wave matrix formulation for multilayered structures is given by Equations (2.19) through (2.26). These equations are based on right-handed (RH) materials. The expressions for reflection and transmission coefficients are identical for dielectric and metamaterials. On the other hand, the phase Φ in Equation (2.26) is preceded by a positive sign for a metamaterial slab and by a negative sign for a dielectric slab [10].

First, the propagation of a parallel-polarized wave in a single metamaterial slab will be studied. To verify that transmission and reflection coefficients computed by the software are correct, the slab in Figure 11 will be used, but this time, with a dielectric constant $\varepsilon_r = -4$. Figure 19 shows transmission and reflection coefficients of the metamaterial slab as a function of frequency. The frequency range covers 500 MHz to 750 MHz. By comparing it with Figure 13 (dielectric panel), over the same frequency range, note that the coefficients are the same.

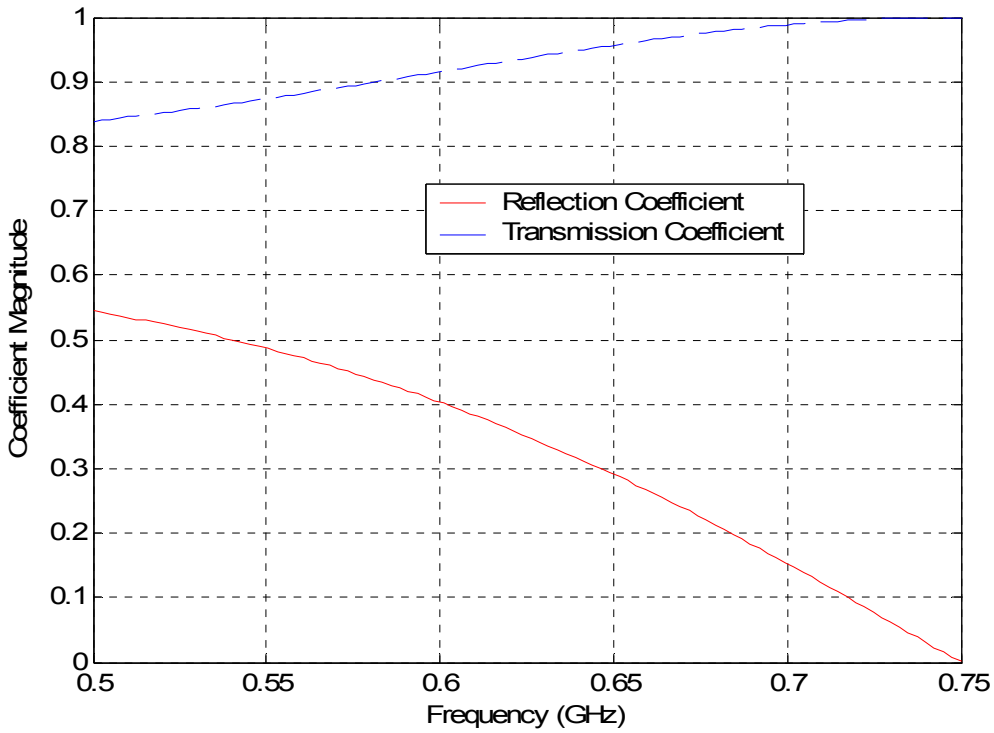

Figure 19. Transmission and reflection coefficients of a metamaterial slab as a function of frequency (normal incidence).

a. Antireflection Coatings

Next, a structure consisting of LH and RH slabs in air (*N*=4) [10] will be studied. Figure 20 shows a pair of metamaterial and dielectric slabs having the same width ($t = 0.1$ m), and opposite permittivities ($\varepsilon_{r_2} = 4, \varepsilon_{r_3} = -4$) embedded in air. In this case, $\Gamma_T = 0$ and $\tau_T = 1$ for any frequency and any angle of incidence.

In Figure 21, the transmission and reflection coefficients of the structure are plotted as a function of frequency for a parallel polarized wave, and Figure 22 shows coefficients as a function of angle of incidence. At 1 GHz, the advantage of structures of alternating slabs is that the total reflection and transmission coefficients are independent of frequency and angle of incidence. Adding new dielectric and metamaterial pairs, which are identical to the first pair, will not change the result. Figure 23 shows the reflection and transmission coefficients for a perpendicularly polarized wave. As evident in the figure, the structure is also polarization independent.

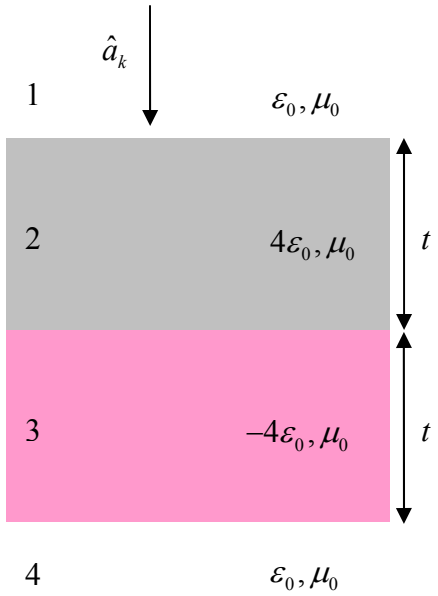

Figure 20. Dielectric and metamaterial slabs embedded in air (antireflection coatings).

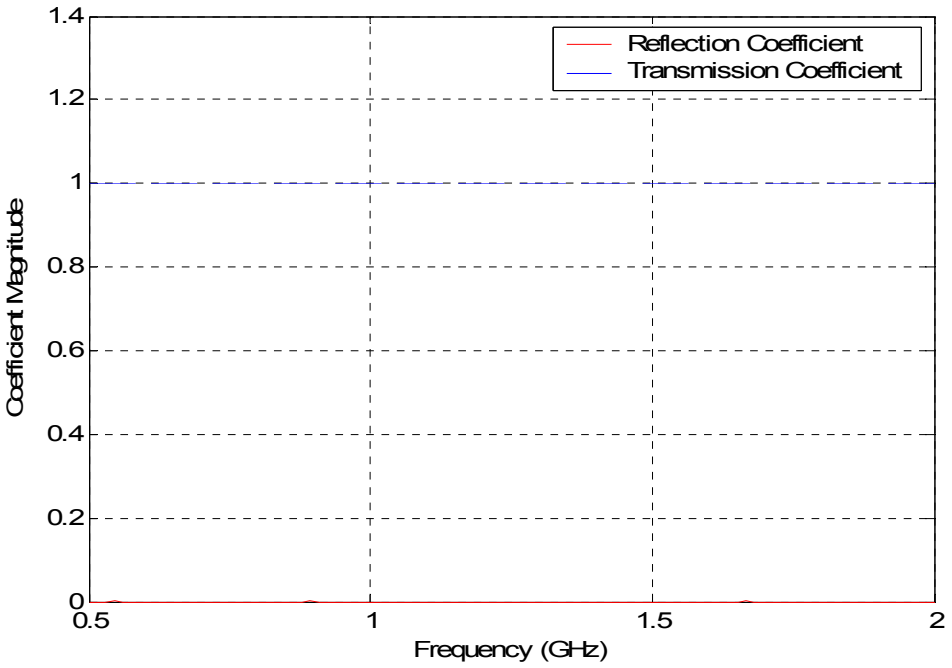

Figure 21. Reflection and transmission coefficients of a pair of dielectric and metamaterial slabs embedded in air as a function of frequency (normal incidence, parallel polarization).

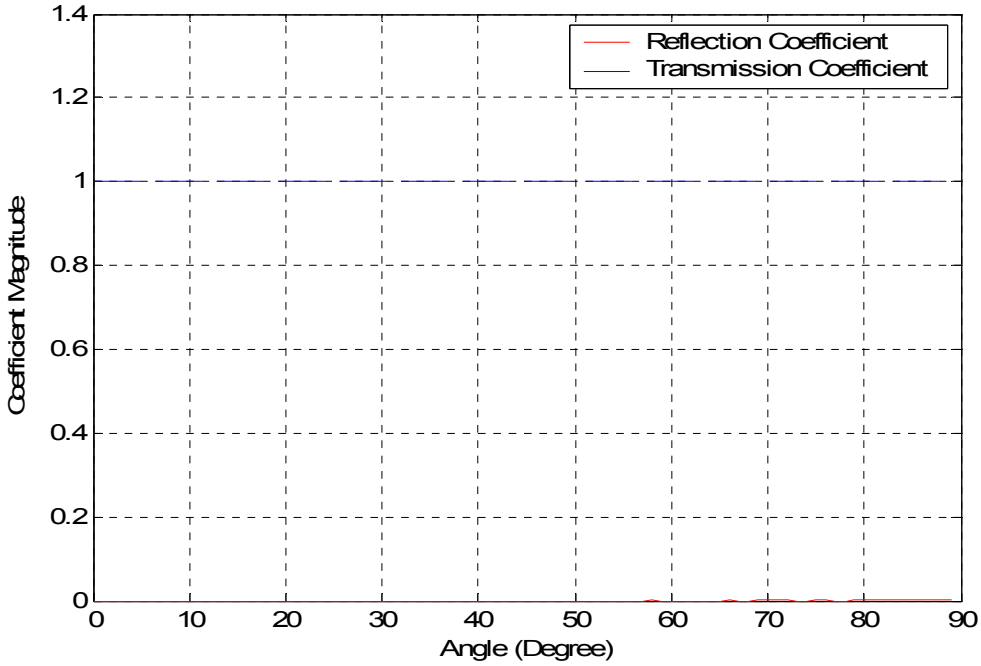

Figure 22. Reflection and transmission coefficients of a pair of dielectric and metamaterial slabs embedded in air as a function of angle of incidence ($f = 1\,\text{GHz}$).

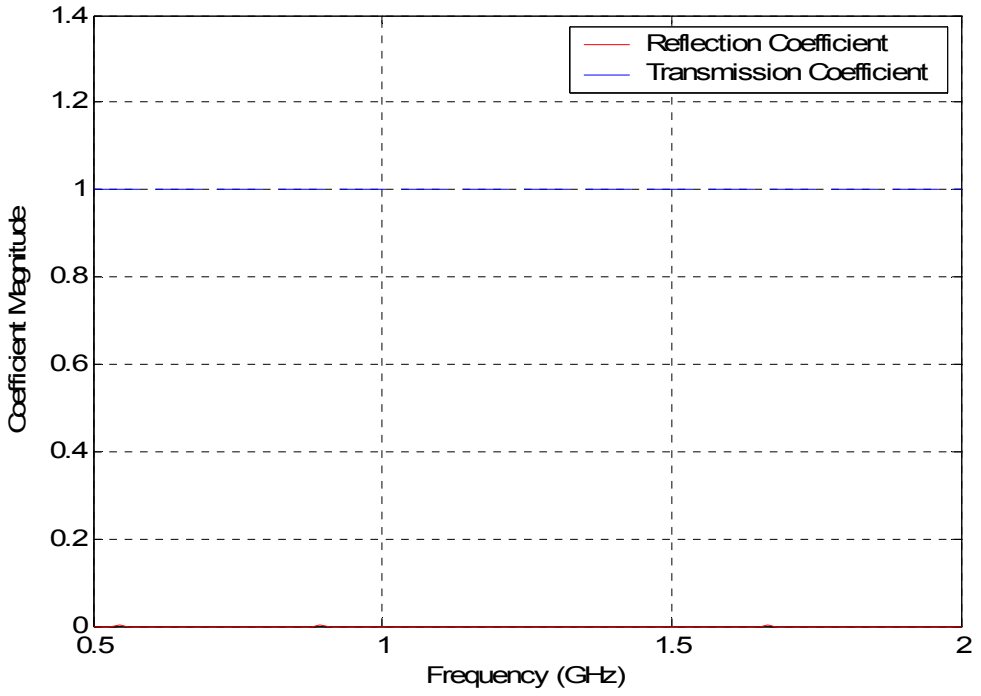

Figure 23. Reflection and transmission coefficients of a pair of dielectric and metamaterial slabs embedded in air as a function of frequency (normal incidence, perpendicular polarization).

The phases of the second and third layers are the same but have opposite signs. From Equation (2.26)

$$\Phi_2 = \frac{2\pi}{\lambda} t_2 \sqrt{\varepsilon_{r_2}\mu_{r_2} - \sin^2\theta_i} \tag{4.14}$$

and

$$\Phi_3 = \frac{2\pi}{\lambda} t_3 \sqrt{\varepsilon_{r_3}\mu_{r_3} - \sin^2\theta_i} \tag{4.15}$$

where $t_2 = t_3$, $\mu_{r_2} = \mu_{r_3}$ and $\varepsilon_{r_2} = -\varepsilon_{r_3}$. Therefore, theoretically the total phase of the structure must be zero. Figure 24 shows the phase of the total transmission coefficient of the structure as a function of frequency. As evident in the figure, the phase of the transmission coefficient is zero except for numerical errors.

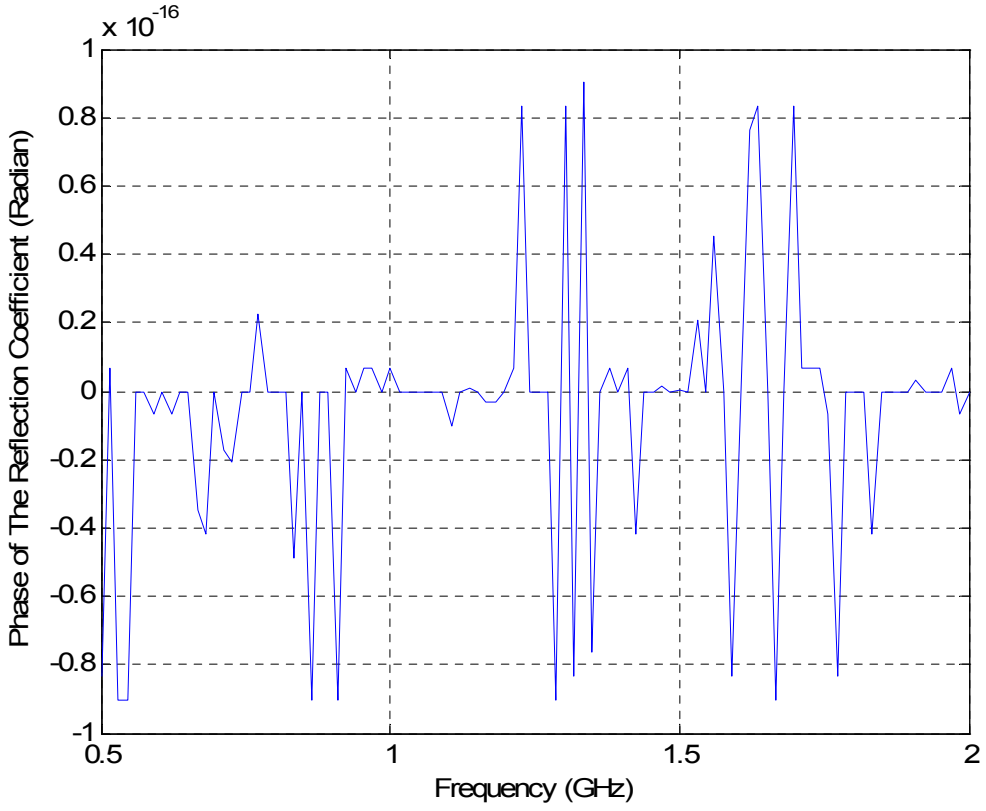

Figure 24. Phase of the total transmission coefficient for a normally incident parallel polarized wave.

b. High-Reflection Coatings

In order to achieve high-reflection, metamaterial and dielectric slabs should be chosen, as given in reference [10]

$$\varepsilon_{r_4} < \varepsilon_{r_3}, \varepsilon_{r_3} > \varepsilon_{r_2}, \varepsilon_{r_2} < \varepsilon_{r_1} \tag{4.16}$$

and $\Phi_2 = \Phi_3 = \pi/2$ at the central frequency. Figure 25 shows a pair of dielectric and metamaterial slabs with different thicknesses that are embedded in air. The permittivities are chosen to maximize the reflection coefficient. In this case, for a wave that is normally incidence, the value of reflection coefficient varies between 0.7 and 0.88 depending on the frequency (Figure 26). At $f = 1.25$ GHz, very high reflection values are achieved for most incidence angles (Figure 27).

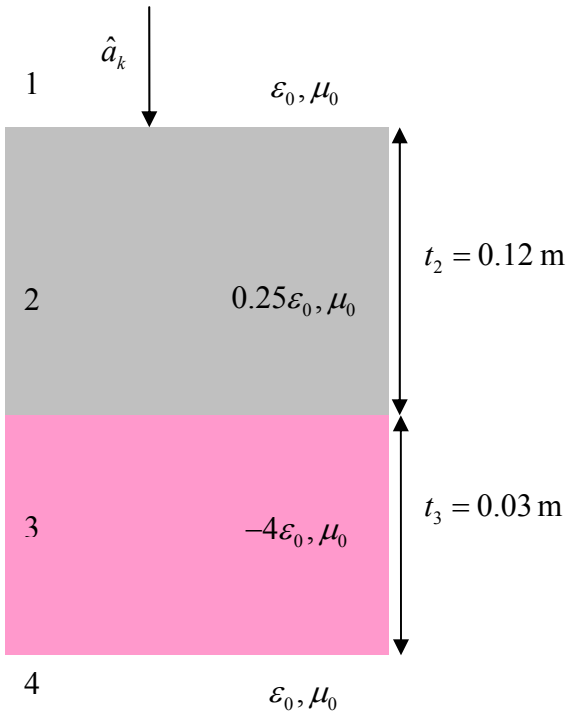

Figure 25. Dielectric and metamaterial slabs with different thicknesses embedded in air (high-reflection coatings).

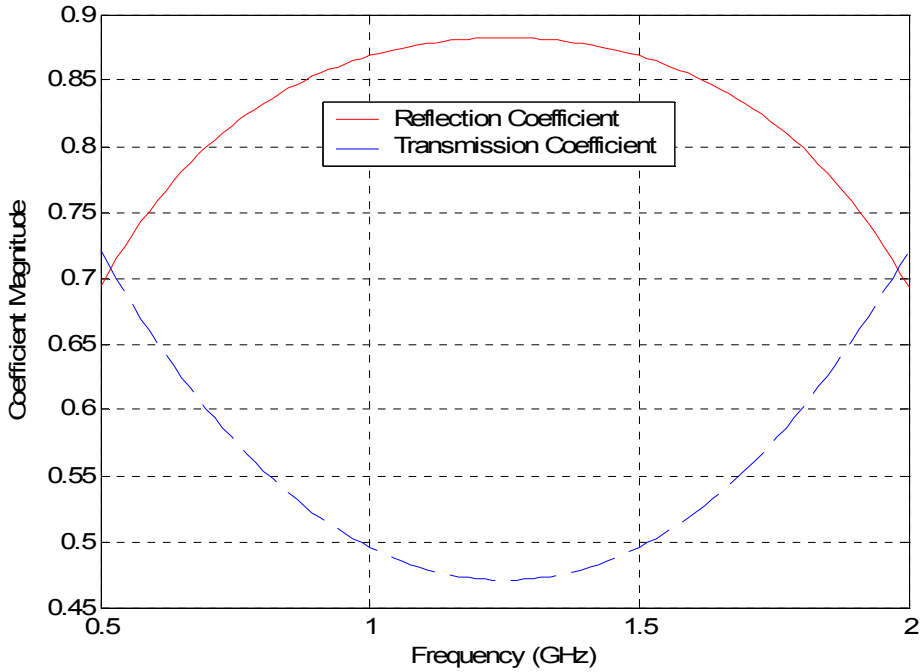

Figure 26. Reflection and transmission coefficients of a pair of dielectric and metamaterial slabs with different thicknesses embedded in air as a function of frequency (normal incidence).

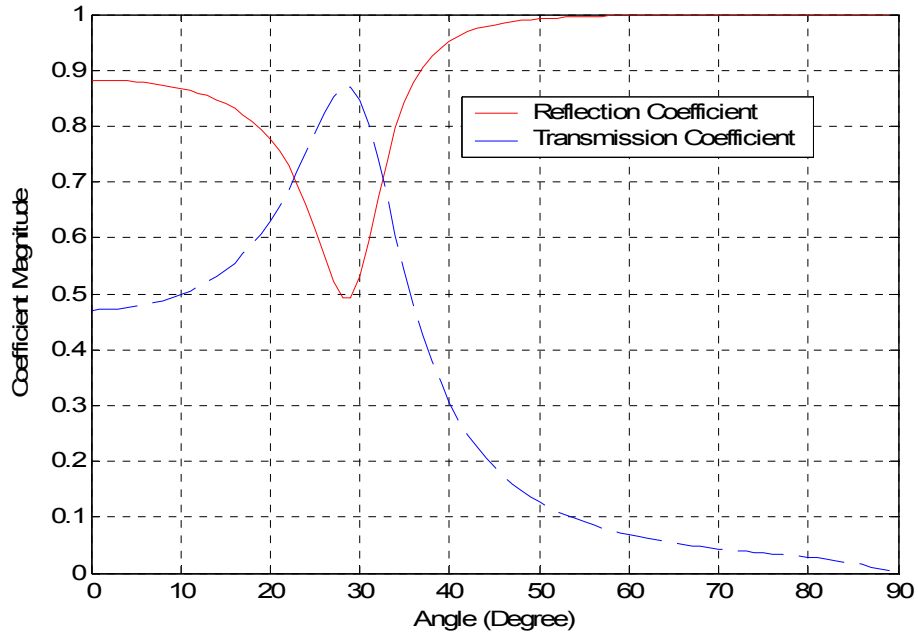

Figure 27. Reflection and transmission coefficients of a pair of dielectric and metamaterial slabs with different thicknesses embedded in air as a function of angle of incidence ($f = 2$ GHz).

4. Pairing an Epsilon-Negative Slab with a Mu-Negative Slab for Zero Reflection

An Epsilon-negative (ENG) medium has negative real permittivity and positive real permeability, while the term mu-negative (MNG) medium is used for the medium, which has negative real permeability and positive real permittivity [11]. It is possible to achieve zero reflection for a pair of ENG-MNG slabs with specific parameters if the incidence wave has a specific angle (Figure 28). Zero reflection is not achievable at other angles of incidence for this pair. The potential application of a matched ENG-MNG pair is ideal image displacement [11]. By placing an object in front of this pair, an observer on the other side of the pair will see the object closer by the amount of the total thickness of the pair.

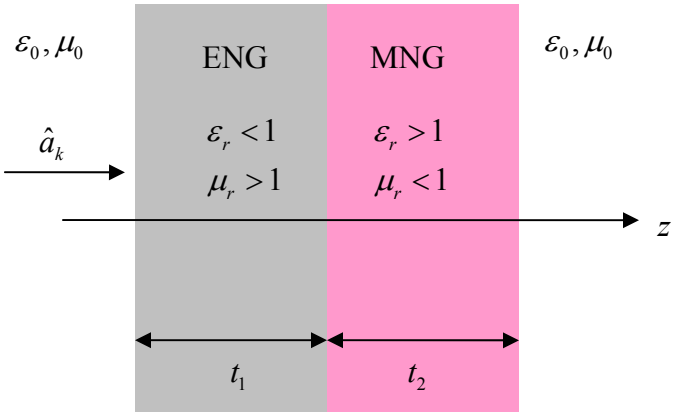

Figure 28. A pair of ENG-MNG slabs for zero reflection.

The parameters for the ENG-MNG slabs are given in Table 1. The propagation constant is given in Equation (2.18). Since with the presence of loss it is not possible to achieve zero reflection due to the mismatch between the slabs, it is assumed that ENG and MNG slabs are lossless. For this matched pair, zero reflection is achieved only for an incidence angle of 45° at $f = 3\,\text{GHz}$ (Figure 29).

	Permittivity (ε)	Permeability (μ)	Thickness (t)
ENG	$-3\varepsilon_0$	$2\mu_0$	$\frac{2\pi}{5\lvert\gamma_{ENG}\rvert}$
MNG	$60\varepsilon_0$	$-43.33\mu_0$	$\frac{2\pi}{4.8\lvert\gamma_{MNG}\rvert}$

Table 1. Parameters for a matched pair of ENG-MNG slabs (thin slabs).

The reflectivity depends more on the total thickness of the structure. The structure is more sensitive to the variation of the incidence angle for a thicker pair (Table 2). Figure 30 shows the reflection coefficient of a thicker pair as a function of the angle of the incidence.

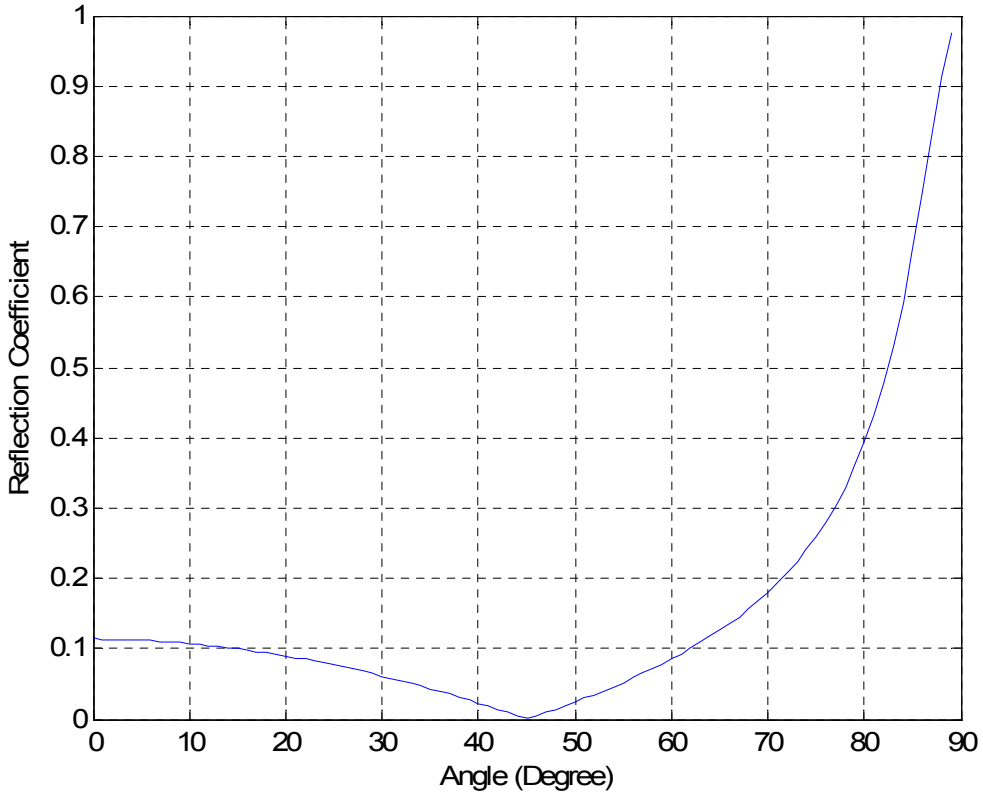

Figure 29. Sensitivity of the reflection coefficient to the variation of the angle of the incidence (thin ENG-MNG slabs).

By comparing Figure 29 and Figure 30, notice that the reflection coefficient remains low for wider range of incidence angles for a thin pair. The reflection coefficient increases rapidly as the angle of incidence deviates from the design angle ($\theta_i = 45^\circ$) in Figure 30.

	Permittivity (ε)	Permeability (μ)	Thickness (t)
ENG	$-3\varepsilon_0$	$2\mu_0$	$\frac{4\pi}{5\lvert\gamma_{ENG}\rvert}$
MNG	$60\varepsilon_0$	$-43.33\mu_0$	$\frac{2\pi}{4.8\lvert\gamma_{MNG}\rvert}$

Table 2. Parameters for a matched pair of ENG-MNG slabs (thick slabs).

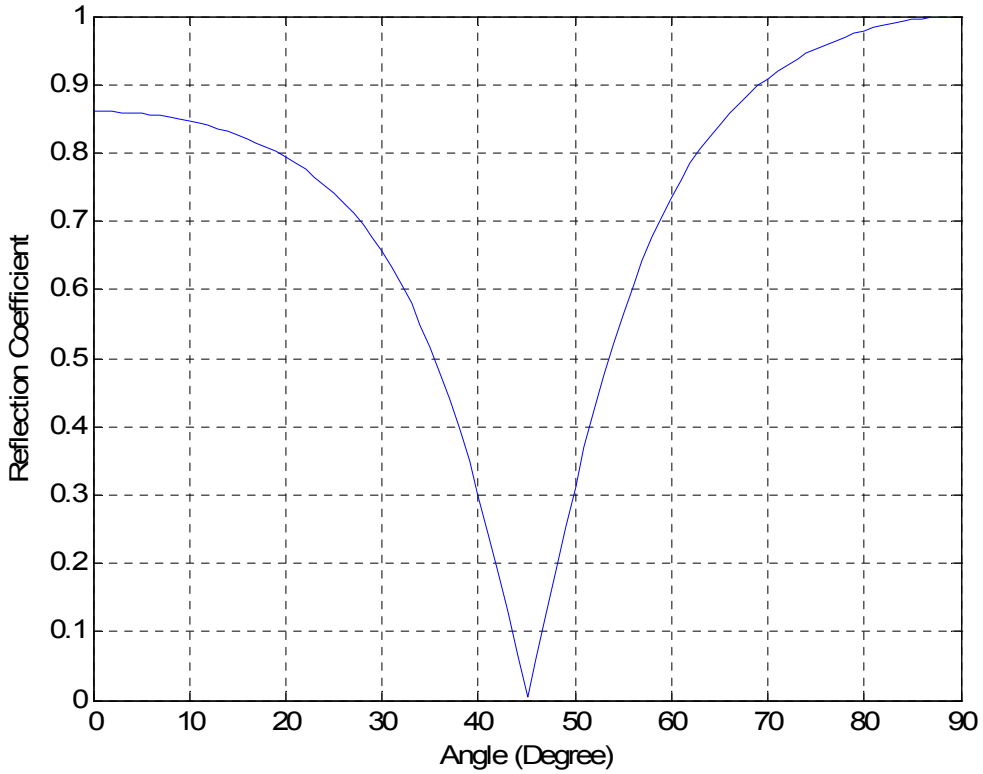

Figure 30. Sensitivity of the reflection coefficient to the variation of the angle of the incidence (thick ENG-MNG slabs).

The potential application of a matched ENG-MNG slab is illustrated in Figure 31. The field distribution at the object plane can be expressed by Fourier components [11]. By selecting the ENG and MNG slab parameters ($\varepsilon_{ENG}, \mu_{ENG}, \varepsilon_{MNG}, \mu_{MNG}$) and thicknesses ($t_{ENG}, t_{MNG}$), the Fourier components tunnel through this matched pair, and the pair becomes transparent [11]. This means that the propagating waves will go through the slab and show up at the exit side with the same magnitude and phase. An observer on the exit side of the pair will see a virtual image of the point source as though it was placed closer by the amount of the total thickness of the slabs ($t_{ENG} + t_{MNG}$). This effect can be used in image reconstruction and resolution enhancement. The planar lenses with negative refraction are described in Chapter III. These lenses create a real image of the source, whereas ENG-MNG pair forms a virtual image.

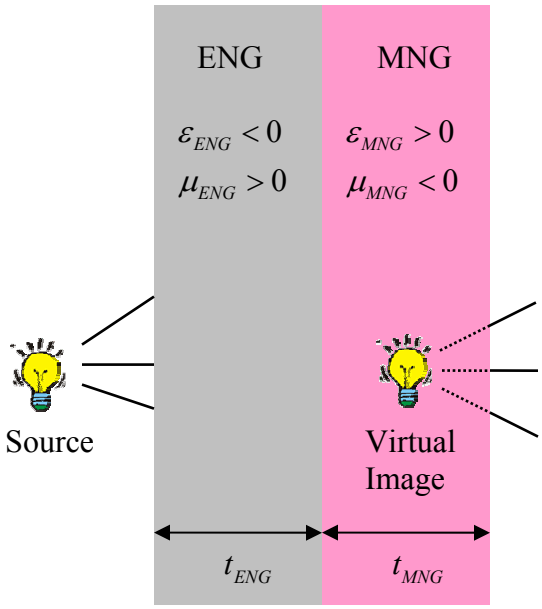

Figure 31. Pair of ENG-MNG layers under certain conditions may provide image displacement and virtual image reconstruction (From Ref. [12])

5. Wet Radome Effect

Water flow due to the rain on the surface of a flat radome may cause a water film up to 1 mil (0.025 mm) thickness. This thin film cannot be seen except from reflections at wide angles. The water layer thickness (t) on a flat panel is given as [13]

$$t = \left(\frac{3RL\mu}{g\rho\cos\theta} \right)^{1/3} \tag{4.17}$$

where L is the plate length, R is the rain rate, μ is the specific viscosity of water, g is the gravitational acceleration, ρ is the density of water and θ is the inclination angle from vertical. The combination of water layer and radome forms a multi-layered structure that can be analyzed using wave matrices. Figure 32 shows transmission loss ($-10\log|\tau|^2$ dB) as a function of water layer thickness for a parallel polarized wave normally incident upon a planar radome and water layer at 20 GHz. The radome consists of a 0.03 in. thick laminate of fiberglass and a water repellent skin of Tedlar [14]. At 20 GHz, the refractive index of the radome is $n = 1.7 - j0.008$ and the refractive index of water [15] is $n = 6.85 - j2.63$. When the radome is present, transmission increases due to the improved impedance match between radome surface and water layer.

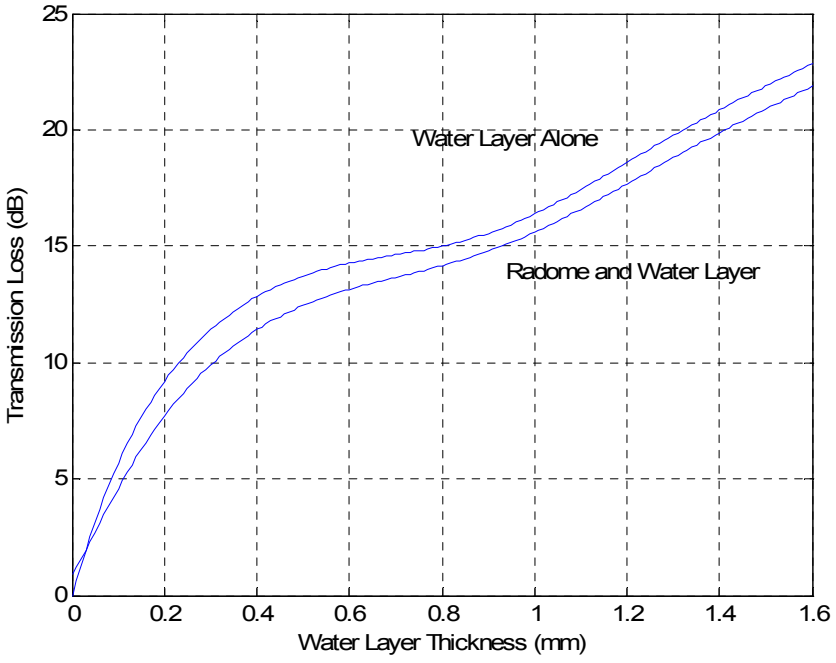

Figure 32. Transmission through radome and water layer as a function of water layer thickness.

In Figure 33, transmission loss as a function of angle of incidence for a 0.032 in. fiberglass radome ($\varepsilon_r = 4$) is plotted at 15.5 GHz. Figure 34 shows the transmission loss

for the same radome with a 0.002 in. water layer ($\varepsilon_w = 49 - j34$). High loss is observed in the case of a water layer.

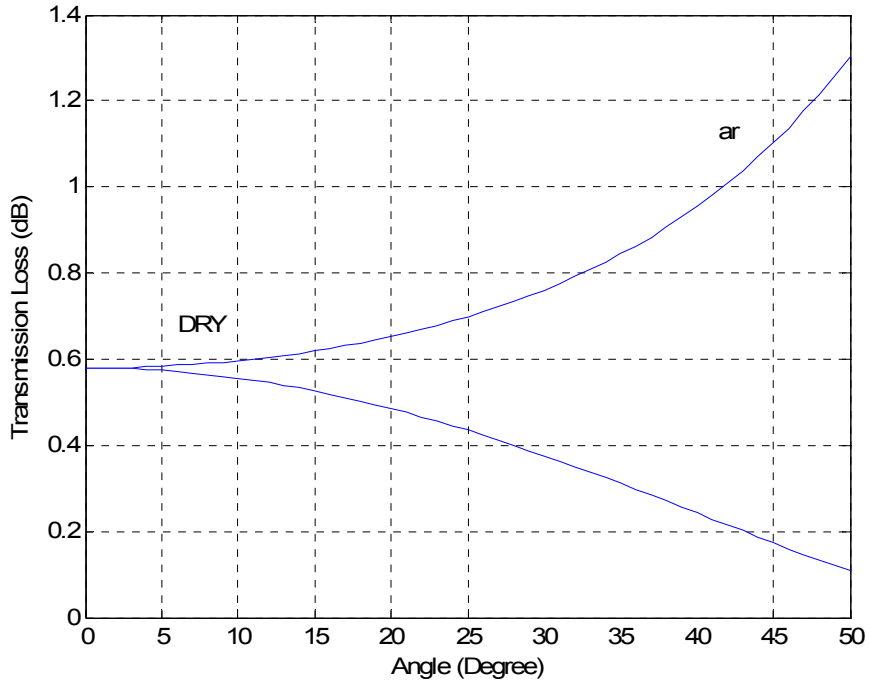

Figure 33. Transmission loss through a fiberglass radome.

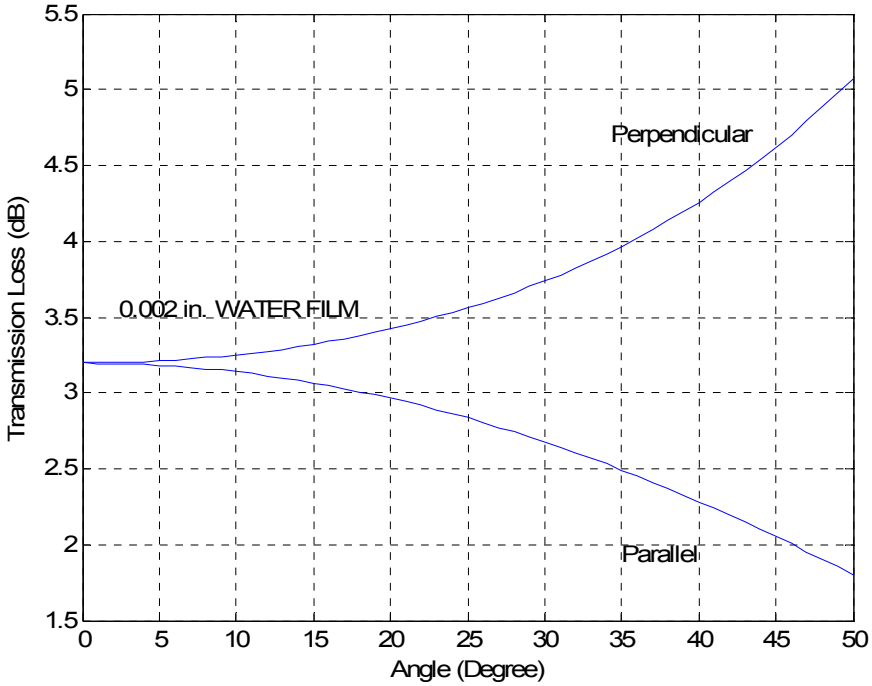

Figure 34. Transmission loss through wet radome.

C. SUMMARY

This chapter is dedicated to simulating the propagation in structures consisting of dielectric slabs, metamaterials or both metamaterial and dielectric slabs. Different methods are described to achieve zero reflection or high reflection. These methods include designing radar absorbing materials, pairing dielectric and metamaterial slabs and pairing an epsilon-negative slab with a mu-negative slab. For all structures, reflection and transmission coefficients are plotted as a function of frequency and angle of incidence. It has been found that all these structures have interesting features. Potential applications of these structures are described, such as reducing RCS of a target or image reconstruction. Finally, transmission through a radome in rain is discussed.

THIS PAGE INTENTIONALLY LEFT BLANK

V. CONCLUSIONS

A. SUMMARY AND CONCLUSIONS

Equations for transmission and reflection coefficients for a single boundary between two dielectric media are presented and the wave matrix approach for layered media described. Unusual properties of metamaterials are discussed and potential applications of DNG materials are presented. Propagation characteristics of planar multilayered structures (including both metamaterial and conventional dielectric layers) are examined by using wave matrix approach.

A combination of dielectric and magnetic material used in RAM applications is examined. The matched characteristic impedance method is used to achieve zero specular reflection, and it has been found that transmission and reflection coefficients are independent of polarization. The conditions for zero specular reflection have been used to validate the MATLAB code.

Anti-reflection coating and high-reflection coating applications have been proposed. It has been found that, for a structure consisting of a pair of metamaterial and dielectric slabs embedded in air having the same width and opposite permittivities, the reflection coefficient is zero and independent of frequency and angle of incidence. These structures could be used as antenna radomes [10]. It has been also found that, by choosing a pair of dielectric and metamaterial slabs with highly concentrated refractive indices, the reflection coefficient is maximized. For one such structure modeled, the reflection coefficient is larger than 0.7 for a large frequency range.

A pair of ENG-MNG slabs has been examined for zero reflection. The variation of the reflection coefficient with angle of incidence is less sensitive for thinner slabs than for the thicker ones. For a thin slab, the reflection coefficient remains low over a wider set of incidence angles. By selecting the ENG and MNG slab parameters and thicknesses properly, the pair becomes transparent to the wave [11]. This effect can be used in image reconstruction and resolution enhancement.

Finally, the effects of rain on transmission through radomes is discussed. It has been found that the existence of rain increases the transmission loss substantially.

B. FUTURE WORK

In this thesis, infinite planar structures consisting of dielectric and metamaterial were examined. No edge effects and no surface or traveling waves were considered. Future research could be conducted to examine the behavior of surface waves and edge diffraction. It would also be interesting to explain how metamaterials could be applied to radar cross section reduction and anechoic chamber design. In principle, absorbing DNG layers could also be used for terminating the computational domain for the finite element (FEM) method and the finite difference time domain (FDTD) method.

APPENDIX. MATLAB CODE

This appendix provides the MATLAB code used to calculate the reflection and transmission coefficients of multi-layered structures in Chapter IV. The code is written in MATLAB 6.5 and based on wave matrices model. This code calculates and plots reflection and transmission coefficients as a function of frequency. It can be modified easily to calculate the coefficients as a function of angle of incidence.

```
%################################################
%SCATTERING FROM MULTI-LAYERED METAMATERIALS
%################################################
%This program calculates and plots refraction and transmission coefficients
%of multi-layered structures as a function of frequency for a specific
%angle of incidence

%INPUTS

%Defining structure properties
clear;
clc;
N = input('Enter the number of layers= ');
fmin=input('Enter Minimum Frequency (GHz)= ');
fmax=input('Enter Maximum Frequency (GHz)= ');
th=input('Enter Incidence Angle (Degree)= ');
p=input ('Enter Polarization Type Parallel (1), Perpendicular (2)=');

%Constants
E0=8.85e-12;       %Permittivity of free space
Mu0=12.5664e-7;    %Permeability of free space
c=1/sqrt(E0*Mu0);  %Speed of light (m/s)

%Defining layer parameters
for layer=1:N ;
   display(layer);
   Mu(layer)=input('Enter Permeability(μ) = ');
   Ei(layer)=input('Enter Permittivity(€) = ');
   t(layer)=input('Enter Layer Length (m) = ');
   sigma(layer)=input('Enter Loss (sigma) = ');
end

f=linspace(fmin,fmax); %Frequency matrix
thr=th*pi/180;         %Angle of incidence (Radian)
```

```
st=sin(thr);
ct=cos(thr);

for i=1:N
   if Ei(i)<0
      E(i)=abs(Ei(i));
   else
      E(i)=Ei(i);
   end
end

%This part calculates the total reflection and transmission coefficients of
%the structure
for k =1:length(f);
   lambda=c/(f(k)*1e9);
   Beta1=2*(pi/lambda);
   total=1;
   w(k)=2*pi*f(k)*1e9;

   %Calculating the characteristic impedance of the layers
   for i=1:N
      Er(i)=E(i)-(j*sigma(i)/w(k)/E0);
      if p==1
         Z(i)=sqrt(Er(i)*Mu(i)-st^2)/Er(i)/ct;
      elseif p==2
         Z(i)=Mu(i)*ct/sqrt(Er(i)*Mu(i)-st^2);
      else
         display ('Polarization type must be 1 or 2');
      end
   end

   %Individual reflection and transmission coefficients of the layers
   ro(1)=(Z(1)-1)/(Z(1)+1);
   tao(1)=ro(1)+1;

   for i=2:N
      ro(i)=(Z(i)-Z(i-1))/(Z(i)+Z(i-1));
      tao(i)=ro(i)+1;
   end

   %Generating wave matrices
   for i =1:(N-1)
      if Ei(i)<0
         sign=-1;
      else
         sign=1;
```

```
        end
        Beta=Beta1*sign;
        A=exp(j*Beta*t(i)*sqrt(Er(i)-st^2));
        Ac=exp(-j*Beta*t(i)*sqrt(Er(i)-st^2));
        total=total*((1/tao(i))*[A,ro(i)*Ac;ro(i)*A,Ac]);
    end

    %Total reflection and transmission coefficients of the structure
    total=1/tao(N)*total*[1 ro(N); ro(N) 1];
    rot(k)=total(2,1)/total(1,1);
    taot(k)=1/total(1,1);
end

%This part plots the coefficients as a function of frequency
plot(f,abs(rot),'r-',f,abs(taot),'--');
grid;
xlabel('Frequency (GHz)');
ylabel('Coefficient Magnitude');
legend('Reflection Coefficient','Transmission Coefficient');
```

THIS PAGE INTENTIONALLY LEFT BLANK

LIST OF REFERENCES

1. Matthew N. O. Sadiku, *Elements of Electromagnetics,* pp. 484-486, Temple University, Philadelphia, 1994.

2. D. Jenn, Notes for EC3630 (Radiowave Propagation), Naval Postgraduate School, 2003 (unpublished).

3. R. E. Collin, *Field Theory of Guided Waves*, pp. 88-91, McGraw Hill, New York, 1960.

4. David R. Smith, "The reality of negative refraction," *Physics World*, May 2003.

5. J. B. Pendry "Negative refraction makes a perfect lens," *IEEE Physics Revolution Letters*, 85, 3966-3969, October 2000.

6. V. G. Veselago, *The Electrodynamics of Substances with Simultaneously Negative Values of* ε *and* μ, Vol. 10, pp. 509-514, 1966.

7. Pendry, Holden, Robbins and Stewart, "Magnetism from conductors and enhanced nonlinear phenomena," *IEEE Transactions on Microwave Theory and Techniques*, Vol. 47, No. 11, November 1999.

8. A. Houck, B. Brock and L. Chuang, "Experimental evolution of a left-handed material that obeys Snell's Law," *Physical Review Letters*, Vol. 90, No. 13, April 2003.

9. D. Jenn, Notes for EC4630 (Radar Cross Section Prediction and Reduction), Naval Postgraduate School, 2003 (unpublished).

10. H. Cory and C. Zach, "Wave propagation in metamaterial multi-layered structures," *IEEE Microwave and Optical Technology Letters*, Vol. 40, No. 6, March 2004.

11. A. Alu and N. Engheta, "Pairing an epsilon-negative slab with a mu-negative slab," *IEEE Transactions on Antennas and Propagation*, Vol. 51, No. 10, October 2003.

12. R. W. Ziolkowski and N. Engheta, "A positive future for double-negative metamaterials," *IEEE Transactions on Microwave Theory and Techniques*, Vol. 53, No. 4, April 2005.

13. J. Chea, "Wet antenna effect on VSAT rain margin," *IEEE Transactions on Comm.*, Vol. 41, No. 8, pp. 1238-1244, August 1993.

14. I. Anderson, “Measurements of 20-GHz transmission through a radome in rain,” *IEEE Transactions on Antennas and Propagation*, Vol. 23, No. 5, September 1975.

15. D. E. Setzer, “Computed transmission through rain at microwave and visible frequencies,” *Bell Syst. Tech. J.,* vol. 49, October 1970.

INITIAL DISTRIBUTION LIST

1. Defense Technical Information Center
   Ft. Belvoir, Virginia

2. Dudley Knox Library
   Naval Postgraduate School
   Monterey, California

3. Chairman, Department of Information Sciences
   Naval Postgraduate School
   Monterey, California

4. Professor David C. Jenn
   Department of Electrical and Computer Engineering
   Naval Postgraduate School
   Monterey, California

5. Professor Michael A. Morgan
   Department of Electrical and Computer Engineering
   Naval Postgraduate School
   Monterey, California

6. Ltjg. Umit Cotuk
   Turkish Navy
   Turkey

7. Deniz Harp Okulu
   Deniz Harp Okulu Kutuphanesi
   Tuzla, Istanbul

8. Hava Harp Okulu
   Hava Harp Okulu Kutuphanesi
   Yesilyurt, Istanbul

9. Kara Harp Okulu
   Kara Harp Okulu Kutuphanesi
   Bakanliklar, Ankara